Quaternary Research 81 (2014) 400–423

Contents lists available at ScienceDirect

Quaternary Research

journal homepage: www.elsevier.com/locate/yqres

Late Miocene–Quaternary rapid stepwise uplift of the NE Tibetan Plateau and its effects on climatic and environmental changes

Jijun Li [a], Xiaomin Fang [b,a,*], Chunhui Song [a,c], Baotian Pan [a], Yuzhen Ma [a,d], Maodu Yan [b]

[a] Key Laboratory of Western China's Environmental Systems, Ministry of Education of China & Research School of Arid Environment and Climate Change, Lanzhou University, Lanzhou 730000, China
[b] Key Laboratory of Continental Collision and Plateau Uplift, Institute of Tibetan Plateau Research, Chinese Academy of Sciences, Beijing 100101, China
[c] School of Earth Sciences & Key Laboratory of Mineral Resources in Western China (Gansu Province), Lanzhou University, Lanzhou 730000, China
[d] Academy of Disaster Reduction and Emergency Management, Ministry of Civil Affairs & Ministry of Education, Beijing Normal University, Beijing 100875, China

ARTICLE INFO

Article history:
Received 6 May 2013
Available online 4 February 2014

Keywords:
Late Miocene–Quaternary
NE Tibetan Plateau
Tectonic uplifts
Yellow River
Climatic and environmental changes

ABSTRACT

The way in which the NE Tibetan Plateau uplifted and its impact on climatic change are crucial to understanding the evolution of the Tibetan Plateau and the development of the present geomorphology and climate of Central and East Asia. This paper is not a comprehensive review of current thinking but instead synthesises our past decades of work together with a number of new findings. The dating of Late Cenozoic basin sediments and the tectonic geomorphology of the NE Tibetan Plateau demonstrates that the rapid persistent rise of this plateau began ~8 ± 1 Ma followed by stepwise accelerated rise at ~3.6 Ma, 2.6 Ma, 1.8–1.7 Ma, 1.2–0.6 Ma and 0.15 Ma. The Yellow River basin developed at ~1.7 Ma and evolved to its present pattern through stepwise backward-expansion toward its source area in response to the stepwise uplift of the plateau. High-resolution multi-climatic proxy records from the basins and terrace sediments indicate a persistent stepwise accelerated enhancement of the East Asian winter monsoon and drying of the Asian interior coupled with the episodic tectonic uplift since ~8 Ma and later also with the global cooling since ~3.2 Ma, suggesting a major role for tectonic forcing of the cooling.

Introduction

The northeastern section of the Qinghai–Xizang (Tibetan) Plateau is the part of the plateau that is most remote from the India–Asia collision zone. In terms of not only the lithosphere and topography but also in climate, this part of the plateau is a transitional zone. In terms of topography, the Tibetan Plateau changes from its highest elevations of 4000–5000 m to lower ones of 2000–1500 m and finally to ca. 1000 m adjacent to the central Loess Plateau and the Gobi deserts. In terms of climate, it lies in the so-called monsoonal triangle zone, which is a transition zone from the Asian monsoon warm-humid climate to inland dry-cold climates (Li et al., 1988). A giant river, the Huang He (Yellow River), arises in this region. The headward incision of the Yellow River has caused not only the formation of a series of terraces but also the complete exposure of Cenozoic basin sediments. Most of these river terraces are covered by thick loess, whereas basin sediments are extremely thick, mostly continuous and bear mammal fossils. These two characteristics allow us to precisely date the river terraces and basin sediments and thereby gain insights into the tectonic uplift of the NE Tibetan Plateau and associated climatic change.

The two endmember dynamic models (thin viscous sheet and extrusion models) predict that the northern plateau was the last to form during simple unidirectional propagation (e.g., Molnar and Tapponnier, 1975; England and Houseman, 1989; Tapponnier et al., 1990, 2001; Meyer et al., 1998; Royden et al., 2008). The stepwise-growth model implies that (1) the present-day northern margin of the plateau formed only in the past few million years and (2) with the northeastward movement of the Altyn Tagh strike-slip fault, the upper crust of the entire NE Tibetan Plateau detached from the lower crust (Burchfiel et al., 1989; Tapponnier et al., 2001), resulting in the progressive northeastern growth of the South, Central and North Qilian Shan (Mts.) (Tapponnier et al., 1990, 2001; Meyer et al., 1998) (Fig. 1).

Fission-track analysis indicates that the Qilian Shan rapidly cooled during the Miocene (Metiver et al., 1998; Jolivet et al., 2001), and preliminary paleomagnetic studies indicate that the Danghe Nan Shan (South Qilian Shan) and western North Qilian Shan may have been uplifted in the Eocene or Oligocene (Yin et al., 2002; Dai et al., 2005). Recent U–Th/He dating of rocks in the central East Kunlun Shan (Mts.) and West Qinling (Mts.) and sedimentological analysis of basins indicate an Eocene–Oligocene deformation and uplift of the NE Tibetan Plateau (Fang et al., 2003; Clark et al., 2010; Lease et al., 2012). Other more recent thermochronologic studies and studies of sedimentary

* Corresponding author at: Key Laboratory of Continental Collision and Plateau Uplift, Institute of Tibetan Plateau Research, Chinese Academy of Sciences, Beijing 100101, China. Tel.: +86 10 8409 7090; fax: +86 10 8409 7079.
E-mail address: fangxm@itpcas.ac.cn (X. Fang).

0033-5894/$ – see front matter © 2014 University of Washington. Published by Elsevier Inc. All rights reserved.
http://dx.doi.org/10.1016/j.yqres.2014.01.002

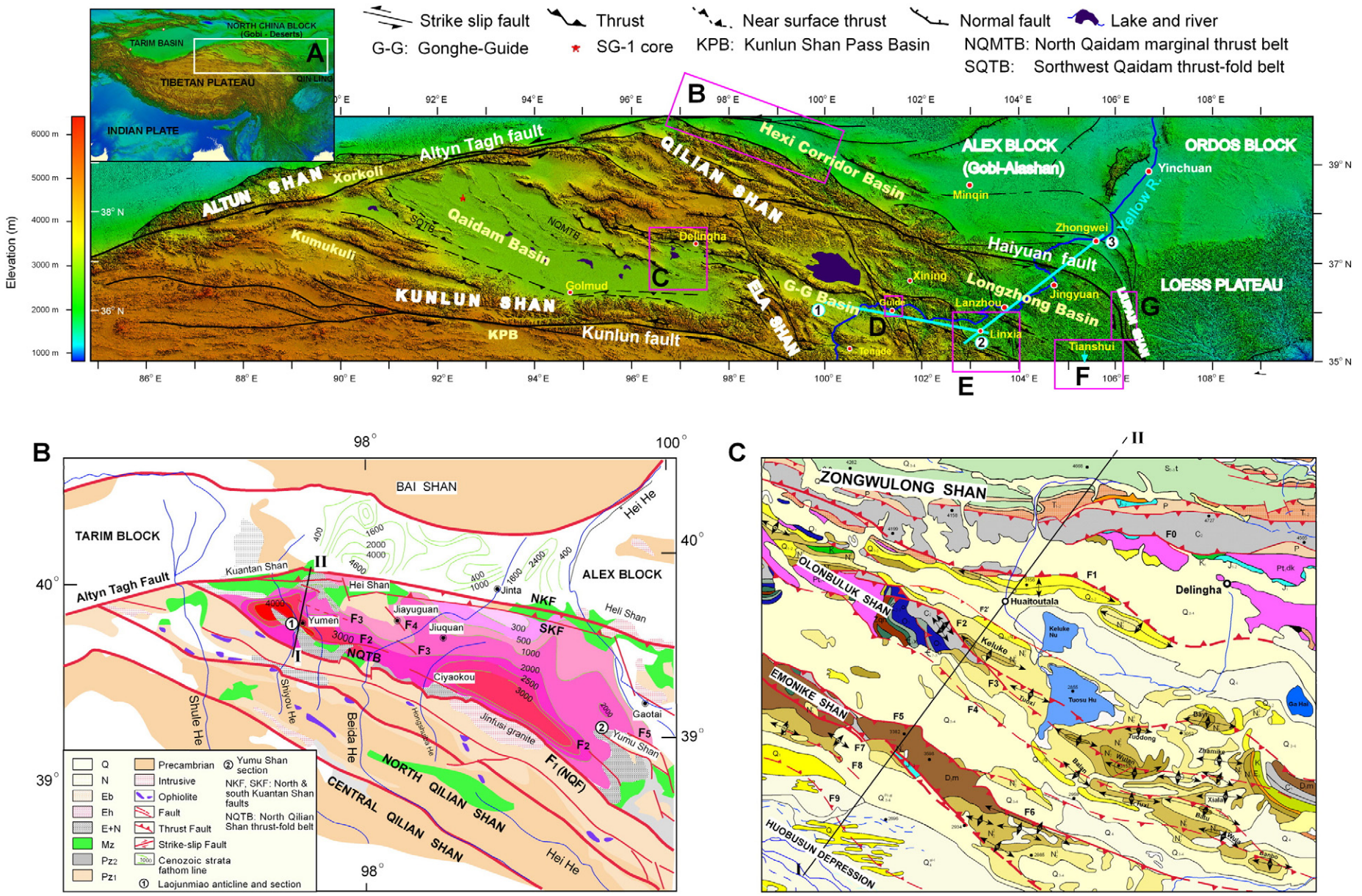

Figure 1. DEM presentation of the geomorphology and major tectonics of the NE Tibetan Plateau, showing the distribution of the mountains and intermontane basins. Insets indicate representative basins for presentation of geologic maps and synthesis in the paper. 1–3: Location of cross-sections along the Huang He (Yellow River) in Fig. 15. b–g: Geologic maps of the Jiuquan Basin, eastern Qaidam Basin, northern Guide Basin, Linxia Basin, Tianshui Basin and Liupan Shan region. Solid red line: surface fault; broken red line: sub-surface fault given by satellite images and seismostratigraphy.

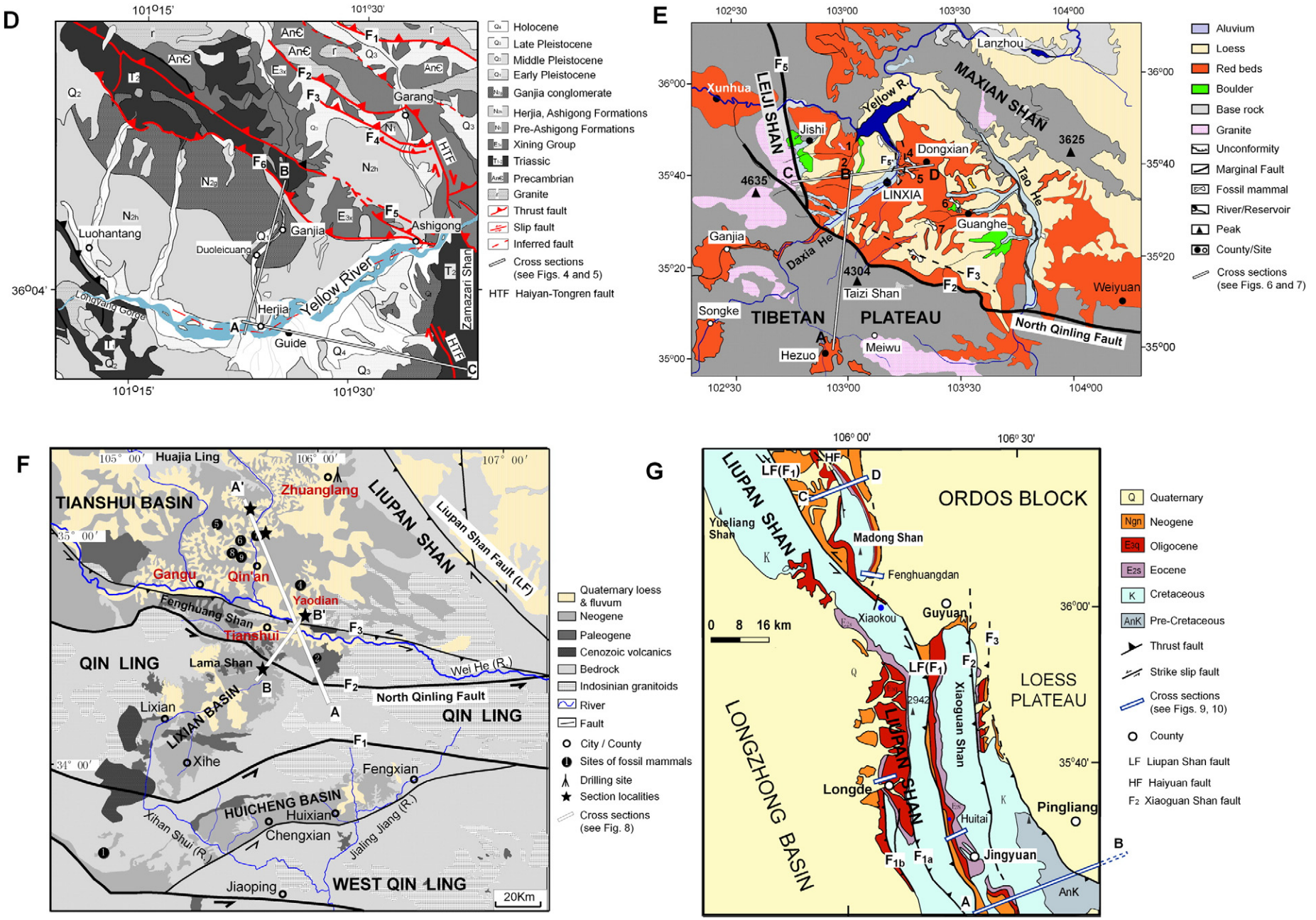

Figure 1 (*continued*).

basins in the NE Tibetan Plateau generally indicate a rapid uplift of the region in the late Miocene and Pliocene (e.g., Molnar, 2005; Enkelmann et al., 2006; Zheng et al., 2006, 2010; Molnar and Stock, 2009; Wang et al., 2012a,b).

Early general conceptual and numerical models indicated that the uplift of the Tibetan Plateau, associated with strong enhancement of erosion and silicate weathering, was responsible for global cooling, monsoon formation and enhancement and drying of the Asian interior (e.g., Ruddiman and Kutzbach, 1989; Broccoli and Manabe, 1992). Recent studies indicate that the growth of the NE Tibetan Plateau may have played an important role in the evolution of the Asian aridification and monsoon climate (e.g., Hövermann and Süssenberger, 1986; An et al., 2001; Liu and Yin, 2002; Dupont-Nivet et al., 2007; Molnar et al., 2010). Although progress has been made on understanding the aridification of the Asian interior, much has been inferred from the red clay–loess/paleosol sequences on the Chinese Loess Plateau. The lack of direct well-dated climatic records from the Asian interior is evident. This has resulted in a range in the interpretations of the drying history of the Asian interior.

A thorough review of all the studies of these broad topics of tectonic uplift of the NE Tibetan Plateau, climatic changes and their interactions is beyond the scope of this paper. Instead, in this limited review, we attempt to synthesise the research efforts of our own group, which has systematically conducted such studies over the last 20 years. To this synthesis, we add new data, identified as such in the text. Many of the findings of these two decades of research have been previously published as isolated studies and only in Chinese (e.g., Burbank and Li, 1985; Li, 1991; Pan et al., 1991, 2009; Li, 1995; Zhu et al., 1996; Fang et al., 1997a,b, 1999, 2003, 2005a,b, 2007, 2012; Li et al., 1997a,b, 2006; Fang and Li, 1998; Ma et al., 1998, 2005a,b; Li and Fang, 1999; Song et al., 2001, 2003).

Here, we generalise regional-scale evidence both in time and space to address when and how the NE Tibetan Plateau reached its present configuration and how this has been coupled with or affected climate. First, we summarise the multiple dating efforts of stratigraphy sequences in representative basins to generalise a chronology of the late Cenozoic stratigraphy in the NE Tibetan Plateau. Second, we synthesise many lines of tectonic evidence in the basins to capture and establish sequences of tectonic events and their deformation and uplift histories. Third, we synthesise climatic records to capture and establish sequences of climatic change events, and finally, we compare the tectonic and climatic events in time and space to determine if a coupling between them exists and what the possible mechanisms might be.

Geologic setting

The NE Tibetan Plateau (~1400 × 400 km = ~560,000 km^2) is tectonically bounded by the sinistral strike-slip Altyn Tagh fault to the west, the sinistral strike-slip Kunlun–West Qin Ling faults to the south, the Qilian–Haiyuan faults to the north and the Liupan Shan transpressional fault to the east (Fig. 1a). It consists of a series of NWW-trending rhombic basins and NWW-directing ranges with high topography (ca. 4000–4500 m in elevation) in the west and low topography (ca. 1500–2000 m) in the east. The main basins and ranges are the Kunlun Shan Pass, Kumukuli, Qaidam, Xorkoli and Hexi Corridor Basins and Kunlun Shan (Shan = Mts.), Altun Shan and Qilian Shan in the west; the Qinghai Lake, Gonghe–Guide and Xining basins and the Anyemaqen, east extending part of the Qilian Shan in the middle; and the Longzhong Basin and West Qin Ling (Ling = Mts.) and Liupan Shan in the east (Fig. 1a).

Two sets of faults border these ranges and basins, in addition to the NE-trending Altyn Tagh envelope fault. The first set, trending NWW–EW, is left-lateral transpressional and plays a major controlling role in the regional tectonics. The second set is NW-trending and right-lateral transpressional. Along the margins of these ranges, various scales of thrust–fold belts are developed, especially along the NWW-trending ranges (Fig. 1a).

The basins received thick accumulations of Cenozoic sediments. These generally thin eastwards (up to 12,000 m in the Qaidam Basin and >4000 m in the Jiuquan Basin in the west, over 2000–1500 m in the Guide and Linxia Basins in the middle, and <1000 m in the Tianshui and Liupan Shan Basins in the east). The overall pattern of the sediments is characterised mostly by three (lower, middle and upper) sets of stratigraphy, often with a clear angular unconformity between the lower and middle sets and mostly a progressive unconformity (growth strata) between the middle and upper sets (Table 1). The lowest set presents an upward-fining sequence of red-purple fine alluvial conglomerates to fluviolacustrine sandstones to mudstones, intercalated with brackish-salt lake or playa marls, gypsums and salts. The middle set also displays a generally upward-fining sequence of mostly brownish alluvial to braided fine river conglomerates–sandstones to brownish red fluviolacustrine sandstones to mudstones, intercalated in the middle to upper parts with greenish–greyish lacustrine mudstones and marls/limestone. The highest set is an upward-coarsening sequence of alternating distinct brownish yellow braided river sandstones to greyish fluvial–alluvial fine to coarse conglomerates and, finally, to boulder conglomerates (Table 1; Figs. 2–10 below). Within the boulder conglomerates are several short-term unconformities. These sequences are exposed, either by the thrust–fold systems in the basin margins or by the Yellow River and its tributaries that have cut into the bedrock (Fig. 1a).

The Yellow River, originating in the Tibetan Plateau, cuts and flows downwards through a series of ranges and basins, forming a set of gorges in the ranges and terraces in the basins. Thick loess sequences cover these terraces (Burbank and Li, 1985; Li, 1991).

Detailed bio-magnetostratigraphic studies in the region provide ages for the exposed basin sediment and terrace loess sequences. These are used to constrain the tectonic and climatic events detected from the formation of thrust–fold systems, basin analysis and river incision histories, as well as sedimentary facies evolution, all relative to the uplift of the NE Tibetan Plateau. For this purpose, six representative basins from different parts of the NE Tibetan Plateau were selected. From west to east, they are the Jiuquan, Qaidam, Guide, Linxia, Tianshui and Liupan Shan Basins, with outlines of the tectonic features and stratigraphic distributions being given in Figure 1 and Table 1.

Stratigraphic chronology

Over the last two decades, our research group has established high-resolution chronologies of stratigraphic sequences in many basins in the NE Tibetan Plateau (e.g., Burbank and Li, 1985; Pan et al., 1991, 2009; Li, 1995; Li et al., 1996, 1997a,b, 2006; Zhu et al., 1996; Fang et al., 1997a,b, 1999, 2003, 2005a,b, 2007, 2012; Fang and Li, 1998; Li and Fang, 1999) (Fig. 2). Most of the research has focused on the middle and upper sets of the Cenozoic basin stratigraphy and used a combination of paleontology, paleomagnetism, ESR, OSL/TL and ^{14}C dating. The middle set of the stratigraphy is predominantly fine sediments and continuous, whereas the upper set is dominated by coarse sediments with several clear and unclear unconformities at different scales of gaps and types (angular and parallel unconformities) (Table 1).

For those basins older than the middle and late Pleistocene, we performed detailed paleomagnetism analyses (mostly sampling at 0.5–2 m intervals, depending on the section thickness and lithology and equivalent to time resolutions of several to ten thousands of years). Measurements were made using a 2G cryogenic magnetometer in a room sheltered from the geomagnetic field after progressive thermal demagnetisation, mostly in 15 to 18 steps from room temperature to 700°C at 10–50°C intervals. After carefully selecting high-precision characteristic remanent magnetisation directions by principal component analysis (setting maximum angular deviation angles to <15°) and passing several paleomagnetic tests (reversal and fold tests),

https://doi.org/10.1016/j.yqres.2014.01.002 Published online by Cambridge University Press

Table 1
Stratigraphic divisions based on bearing fossil mammals and paleomagnetic dating for the studied basins in the NE Tibetan Plateau.

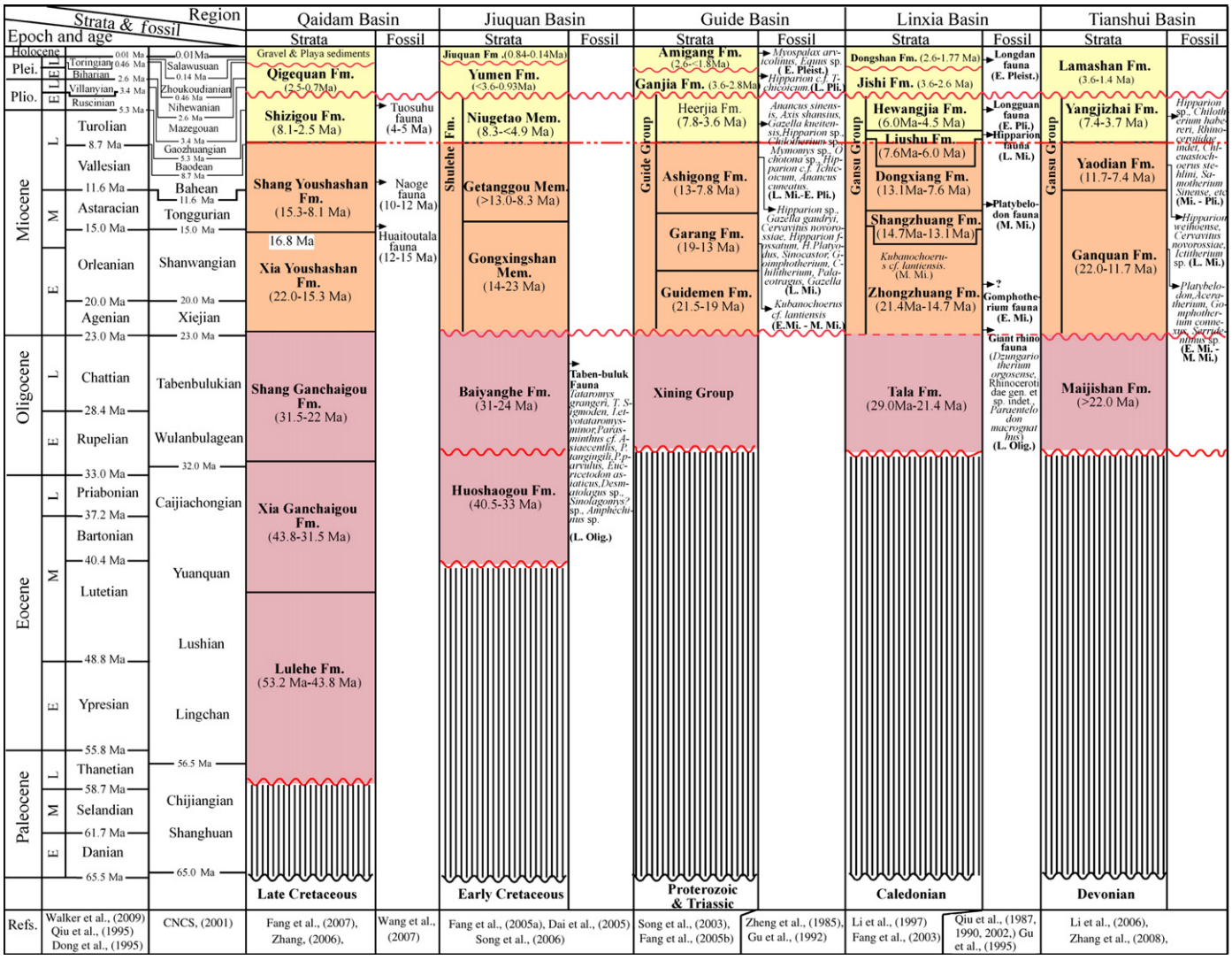

high-quality of magnetic polarity zones were obtained for all the measured sections.

In cases for which the preliminary correlations of the observed polarity zones with the geomagnetic polarity time scales (GPTS) suggested that we had taken samples from weathered surfaces, we resampled sections in the field. Analysis of these new samples improved the quality of the obtained polarity zones for most sections. These high-quality and high-resolution polarity zones can be well-correlated with the GPTS, based on constraints in the framework provided by many layers of fossil mammals found in the measured sections or in other equivalent strata in the basin (Fig. 2 and Table 1). Details for our paleomagnetic method and correlations have been given in many papers written by members of our group.

Here, we summarise these magnetostratigraphies for six representative basins (Fig. 2). For those basins younger than the middle and late Pleistocene, a combination of ESR, OSL/TL and organic ^{14}C dating were applied, especially for the loess–paleosol sequences. These analyses help to constrain younger river terrace ages and stratigraphic unconformities. In combination, these multiple dating methods have determined the 1960-m-thick Laojunmiao section (97°32′E, 39°47′N) along the Laojunmiao anticlines in the Jiuquan Basin (Fig. 1b) to be <13 Ma. The ages of the Getanggou and Niugetao Members in the Shulehe Fm. and the Yumen, Jiuquan and Gobi Fms. are >13–8.3 Ma, 8.3–4.9 Ma, 3.66–0.93 Ma, 0.84–0.14 Ma and 0.14–0 Ma, respectively (Fang et al., 2005a) (Table 1, Fig. 2b). The 4570-m Huaitoutala section along the northern limb of the Keluke anticline against the northern edge of the Olonbuluk Shan in the eastern Qaidam Basin (Fig. 1c) is ~15.7–1.8 Ma, with ages of >15.7–15.3 Ma, 15.3–8.1 Ma, 8.1–2.5 Ma and 2.5–<1.8 Ma, respectively for the Xia Youshashan, Shang Youshashan, the Shizigou and Qigequan Fms. (Fang et al., 2007) (Table 1, Fig. 2a). The >1400-m Amigang–Ganjia sections in the Guide Basin (Fig. 1d) are ~11.5–1.8 Ma, with ages of >12–7.8 Ma, 7.8–3.6 Ma, 3.6–2.6 Ma and 2.6–1.8 Ma for the Ashigong Fm., Herjia Fm., Ganjia Fm. and Amigang Fm., respectively (Fang et al., 2005b; Yan et al., 2012b) (Table 1, Fig. 2c). The >700-m Wangjiashan–Dongshanding sections in the east limb of the Yinchuangou anticline in the Linxia Basin (Fig. 1e) are >11–0 Ma, with ages of ~13–7.6 Ma, 7.6–6 Ma, 6–4.5 Ma, 3.6–2.6 Ma, 2.6–1.75 Ma, 1.75–1.72 Ma and 1.72–0 Ma for the Dongxiang, Liushu, Hewangjia, Jishi, Dongshan and Jinggoutou Fms. and loess–paleosol sequence, respectively (Li, 1995; Fang et al., 1997a, b, 2003; Li et al., 1997b) (Fig. 2d). The Lamashan, Yaodian and Yanwan sections in the central and southern Tianshui Basin (Fig. 1f) are >17.1–2.6 Ma, with ages of ~17.1–11.7 Ma, 11.7–7.4 Ma, 7.4–3.7 Ma and 3.4–2.6 Ma for the Ganquan Fm., Yaodian Fm., Yangjizhai Fm. and Lamashan Fm., respectively (Li et al., 2006; Wang et al., 2012a,b; Zhang et al., 2013a,b) (Table 1, Figs. 3a–c). Finally, the

https://doi.org/10.1016/j.yqres.2014.01.002 Published online by Cambridge University Press

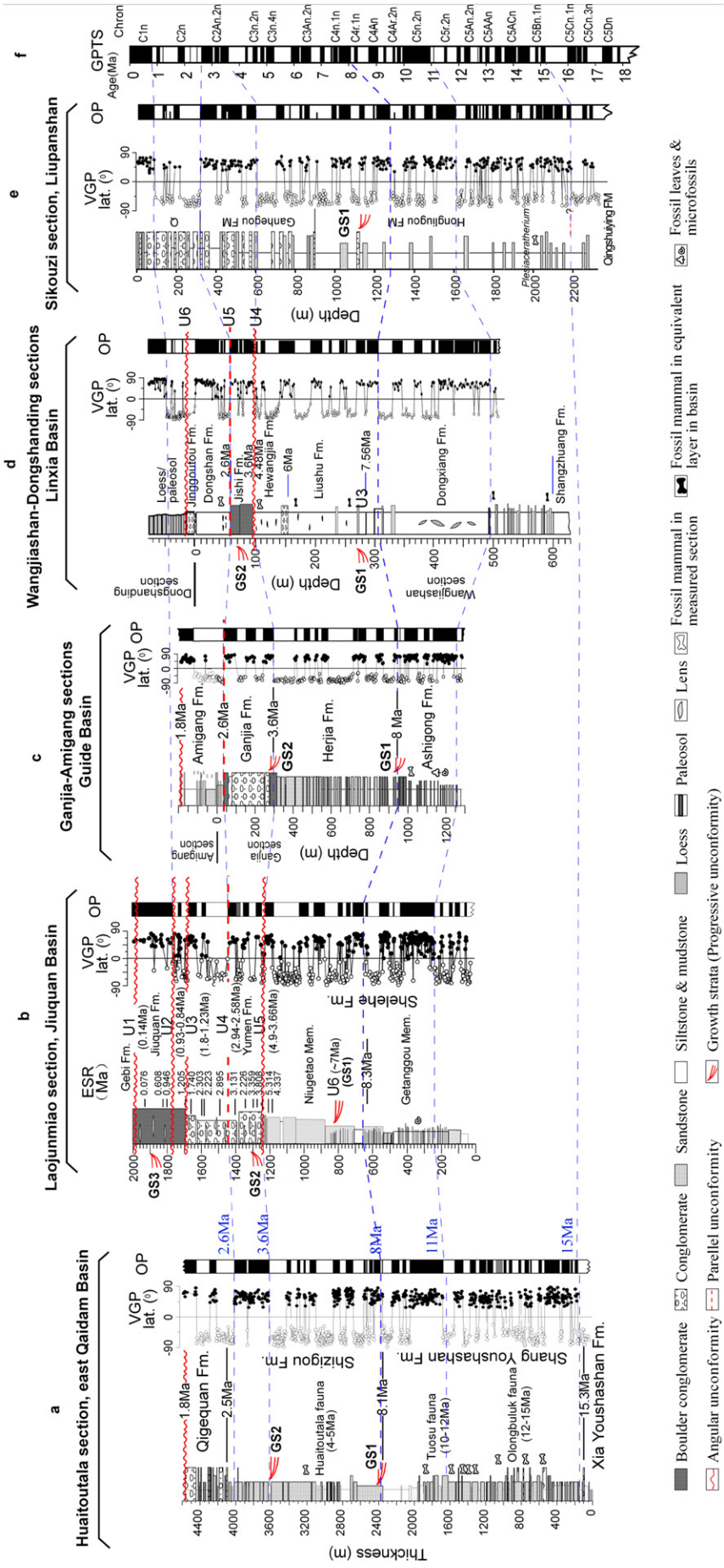

Figure 2. Comparison of high quality and resolution of magnetostratigraphic sections from representative basins in the NE Tibetan Plateau. The summarised lithology and stratigraphic evolution are plotted for an overview of how the basin stratigraphic sequences record the deformation and uplift of the NE Tibetan Plateau from the west to east of the studied region (see Fig. 1 for locations). For fossil mammals, please see Table 1. GPTS: Geomagnetic polarity time scale of Cande and Kent (1995).
Huaitoutala, Laojunmiao, Ganjia–Amigang and Wangjiashan–Dongshanding sections compiled from Fang et al. (1995, 2003, 2005, 2007), Li et al. (1996) and Li and Fang (1999). Sikouzi section modified from Wang et al. (2011a,b).

https://doi.org/10.1016/j.yqres.2014.01.002 Published online by Cambridge University Press

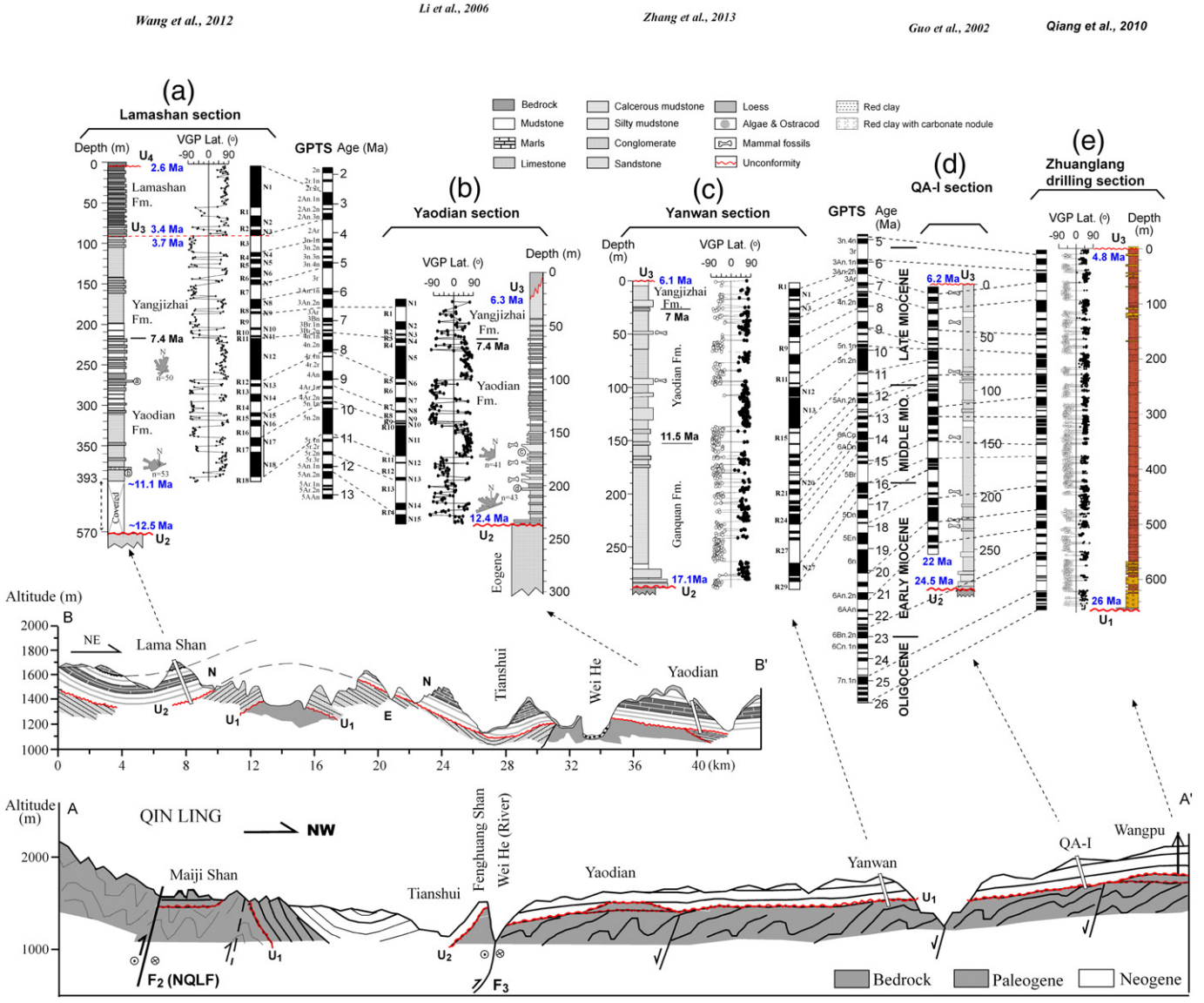

Figure 3. Bottom: Cross sections A–A′ and B–B′ in Fig. 1f from the West Qin Ling to the Tianshui Basin, showing the tectonogeomorphologic–sedimentologic relationships between the basin and the mountains and locations of the Lama Shan, Yaodian, Yanwan and QA-I sections and the Zhuanglang borehole. Upper: Magnetostratigraphy of the Lama Shan (a) (Wang et al., 2012a,b), Yaodian (b) (Li et al., 2006), Yanwan (c) (Zhang et al., 2013) and QA-I sections (d) (Guo et al., 2002) and the Zhuanglang borehole (e) (Qiang et al., 2011). GPTS: Geomagnetic polarity time scale of Cande and Kent (1995). Note our dating of the stratigraphy in the three sections agrees well not only with the fossil mammal suggested ages (Table 1) but also with previously dated sequences (d, e) in the region and the borehole in the northern part of the basin (Guo et al., 2002; Qiang et al., 2011).
The bottom panel is redrawn from Wang et al. (2012a,b).

Shenyu section in the Shengyu Basin, on the east limb of the southern Liupan Shan, is ~8.1–3.4 Ma (Figs. 1g and 4b), and the Sikouzi section on the east limb of the northern Liupan Shan is >17 Ma to <0.4 Ma (Figs. 1g, 2e).

Evidence of tectonic deformation and uplift of the NE Tibetan Plateau

Growth strata and unconformity

Growth strata mark a progressive unconformity and are characterised by a set of syn-tectonic depositional stratigraphy developed at the limb-top and fronts of a growth fold in a thrust–fold system of the foreland basin (e.g., Suppe et al., 1992; Rafini and Mercier, 2002; Verges et al., 2002). These growth strata directly record the details of tectonic deformation. They occur in an obvious triangle shape called a "growth triangle" that can be quantified (Suppe et al., 1992). We propose here a formula to roughly quantify a rate for the growth strata (G) by simple measurement of the change of the angle of the growth triangle expressed either as sediment thickness T_s divided by the horizontal projection of the limb length L_h or as the growth angle difference $\delta(\theta)$ divided by the growth time $\delta(t)$ as follows (Fig. 5):

$$G = \delta(\theta)/\delta(t). \quad (1)$$

If folding uplift keeps a consistent rate, $\delta(\theta)$ will be constant, forming a set of recognisable growth strata (Fig. 5IIa). Accelerating thrusting and folding will result in reduced or thickened thickness of sediments deposited on the top of or in the down-slope of the fold and will also increase the corresponding growth angle θ (Fig. 5IIb). If thrusting and folding are too fast, deposition on the top of the fold will not occur. Instead, it will be subject to erosion, forming a parallel or angular unconformity depending on the folding and erosion rates. In this case, a retreat-depositional sequence will be formed (Fig. 5IId). Reversing these processes will accelerate deposition on the top of the fold, and

https://doi.org/10.1016/j.yqres.2014.01.002 Published online by Cambridge University Press

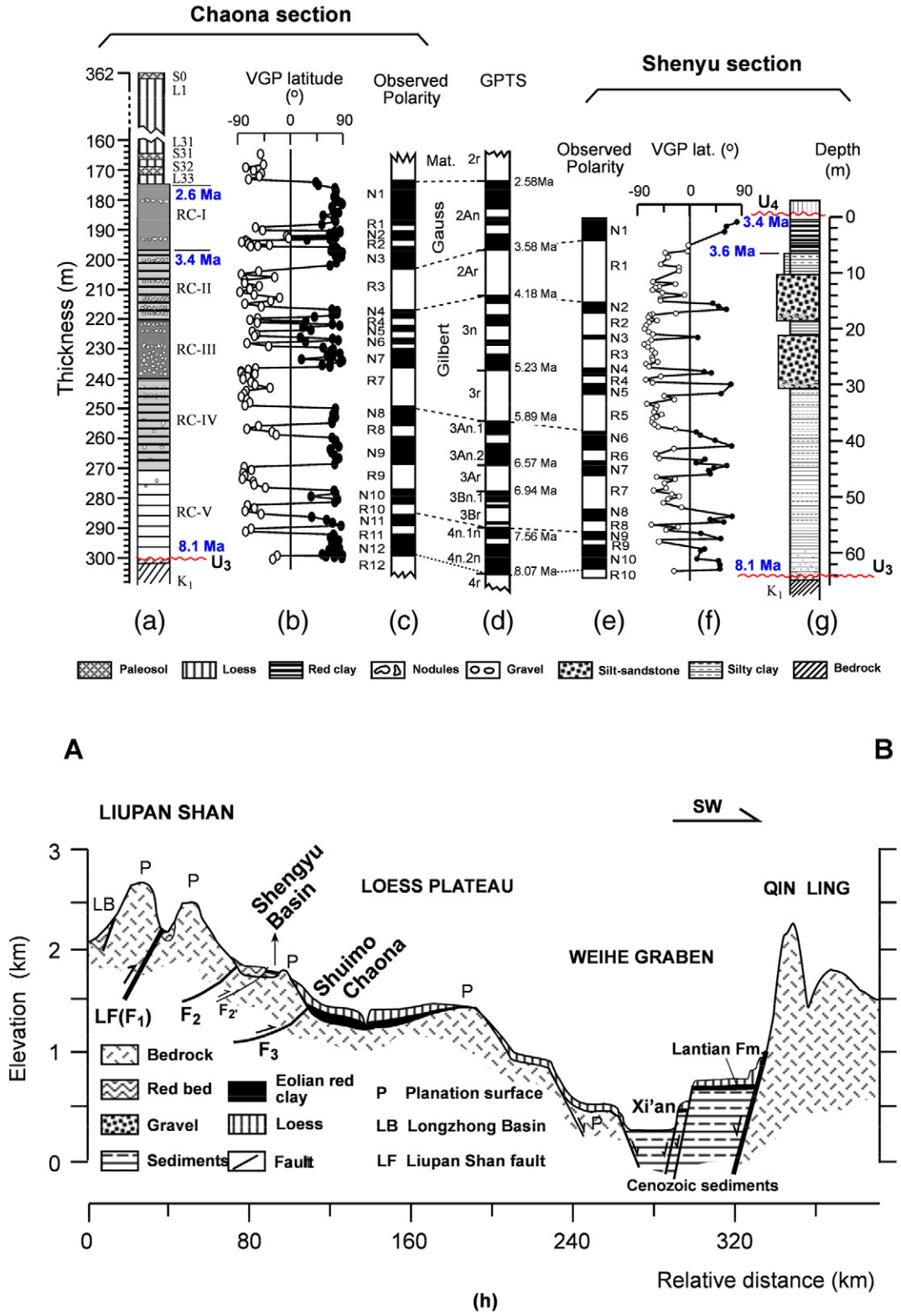

Figure 4. Bottom: Cross Section A–B in Fig. 1g from the Liupan Shan to West Qin Ling, showing the tectonogeomorphologic relationships between the Liupan Shan, the Loess Plateau, the Weihe Graben and the West Qin Ling and the locations of the Shengyu and Chaona sections (h). Note the propagation fault F2′ lifted early Cenozoic red beds and bedrock and formed the small Shengyu Basin in its front. Upper: Magnetostratigraphy of the Chaona (a–c) and Shengyu sections (e–g). GPTS: Geomagnetic polarity time scale of Cande and Kent (1995). Redrawn from Song et al., 2001.

an onlap stratigraphic sequence will be formed (Fig. 5IIc). Thus, recognition and continuous quantification of growth strata can provide great information on the time, rate and style of deformation in relation to thrusting and folding in a foreland basin (Suppe et al., 1992; Ford et al., 1997; Rafini and Mercier, 2002).

Detailed measurements of stratigraphic dips and chronology of the Laojunmiao section along the northern limb of the Laojunmiao anticline in the Jiuquan Basin in this paper clearly indicate that there developed three large sets of strata growth (GS1 to GS3) and five unconformities U_1 to U_5 that are between or within the growth strata (Fig. 6). GS1

https://doi.org/10.1016/j.yqres.2014.01.002 Published online by Cambridge University Press

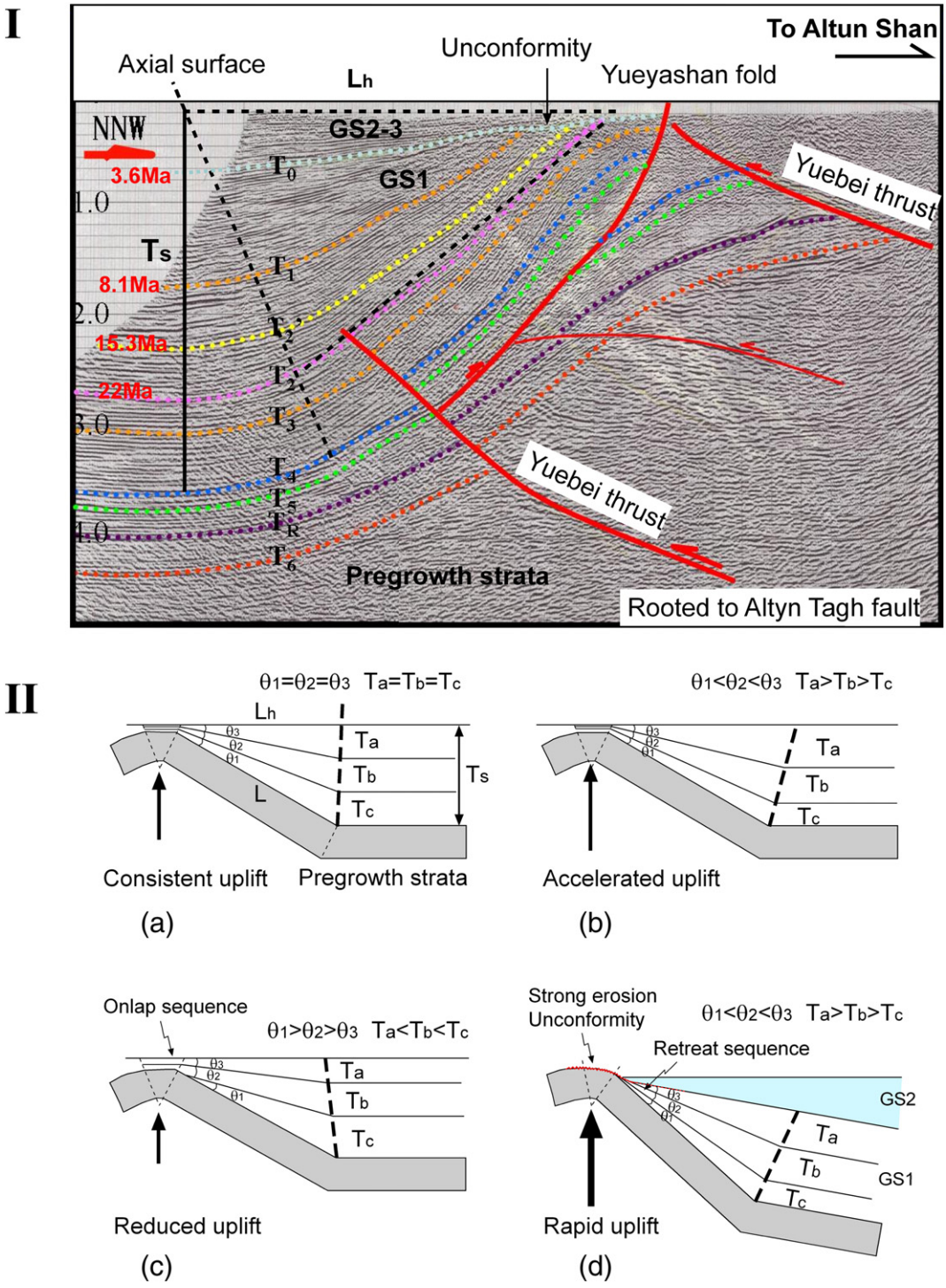

Figure 5. Upper: Seismostratigraphy along the western margin of the Qaidam Basin and eastern slope of the Altun Shan showing the occurrence of two sets of the growth strata, separated by an angular unconformity at hanging side, caused by growth faults rooted from the Altyn Tagh strike slip fault. Bottom: Schematic diagrams showing the relationships between uplift rate and development of growth strata and its associated unconformity and stratigraphic sequence.

began to develop in the lower part of the Niugetao Member near the thickness of 750 m at ~7.4 Ma, and ended at the thickness of 1206 m at ~4.9 Ma where the dips change rapidly from 84° to 63° within a short distant or time period (2.4 Ma; growth rate G = 8.75°/Ma, using formula (1)) (Fig. 6b). GS2 began and ended at the thicknesses of 1206 m (~4.9 Ma) and 1713 m (~0.93 Ma), respectively, with corresponding dips changing from 55° to 25°. The angular unconformity (U_5) is accompanied with the beginning of GS2, where the dips change abrupt from 63° to 55° below and above the unconformity.

The chronology indicates that U_5 was formed between ~4.9 Ma and 3.66 Ma (Fang et al., 2005a). Thus the growth rate G of the GS2 is calculated at 11°/Ma (Fig. 6).

GS3 also begins with an unconformity: U_2, having abrupt dip changes from 25° in strata below U_2 to 15° above, over a time interval of ~0.09 Ma, at ~0.93–0.84 Ma. GS3 straddles the stratigraphic intervals from the thicknesses of 1713 m to 1940 m (0.15 Ma) with dips changing from 15° to 6° (Fig. 2b). The calculated growth rate G is ~13°/Ma. Thus, the development of GS1 to GS3, as quantified by the

https://doi.org/10.1016/j.yqres.2014.01.002 Published online by Cambridge University Press

change (increasing) of G, clearly indicates accelerated folding and upheaval.

Seismostratigraphy across the North Qilian Shan thrust–fold belt (NQTB) in the Jiuquan Basin from this paper confirms the occurrences of the three sets of growth strata (GS1 to GS3) above (Figs. 6c, d; see Fig. 1a for locations). GS1 starts clearly in the lower part of the Niugetao Fm. (N_2n), GS2 at the beginning of the Yumen Conglomerate Bed traditionally classed as the Quaternary (Q_1y), but now paleomagnetically dated to ~3.66 Ma (Figs. 2b and 6b), and GS3 starts with the Jiuquan Conglomerate Bed (Q_2j) and superimposes unconformably on GS2 (Figs. 6c, d).

In the Qaidam Basin, we newly recognised three sets of growth strata GS1 to GS3 from both outcrops and seismostratigraphy (Fig. 5I). GS1 starts at the Shizigou Fm. (N_2^3) at ~8.1 Ma, GS2 was formed at 3.6–1.8 Ma in the Huaitoutala outcrop section with the end of the Kuluke anticline at ~1.8 Ma, but it may continue to ~0.8 Ma in the seismostratigraphy in other parts of the folds (figures are not presented here). GS3 is hard to observe in outcrop as most of the stratigraphy has not been thrusted or folded and exposed. However, in the outcrop, we can see that the Kuluke anticline is top-truncated by a remarkable unconformity in the sequence and geomorphologic position that is equivalent to the unconformity U_2 in the Laojunmiao section at ca. 0.93–0.84 Ma (Fig. 2). Superimposed on this unconformity is a thick uncemented gravel bed of alluvial fans (figure is not presented here). This unconformity and its overlying uncemented gravel bed are widely distributed in the basin margins.

At Huatugou in the western Qaidam Basin, this unconformity was dated to the middle Pleistocene using ESR and cosmogenic methods (Ren et al., 2006). Our new data show that these three sets of growth strata exist not only widely in the north Qaidam marginal thrust belt (NQMTB) along the southern margin of the Qilian Shan (Fig. 6) but also in the thrust belt of the Altyn Tagh fault in east slope of the Altun Shan and western margin of the Qaidam Basin (Fig. 5I). Furthermore, a striking angular unconformity presents between GS1 and GS2 along the margin of the Altun Shan (Fig. 5I). The rates of the three growth strata increase considerably upwards from 1.8–2°/Ma (GS1) to 5.6–7.5°/Ma (GS2–3) (Fig. 5I). This evidence not only indicates that the Qilian Shan, Kunlun Shan and Altun Shan have experienced roughly the same episodes of tectonic deformation and uplifts in the late Miocene–Quaternary but also indicates that the uplift processes accelerated with time.

In the Gonghe–Guide Basin, field views and dip measurements of the completely exposed great cliff cross-section of the Nongchun River, from Herjia at the side of the Yellow River to Ganjia at the front of the Laji Shan, can easily demonstrate a progressive southward shallowing of stratigraphic dips toward the basin. The change of dip is not so significant south of the measured Ganjia section but is significant to its north, indicating that the measured section is just located along the axial surface of the growth strata (figure is omitted). By dip changes and their clustering nature, roughly two sets of the growth strata (GS1 and GS2) can be recognised. GS1 began at about the onset of the fine conglomerate (Herjia Fm.) at ~7.8 Ma (G = ~4.6°/Ma). GS2 began at the boulder conglomerate of the Ganjia Fm. at ~3.6 Ma and lasted to the end of the lake sediments of the Amigang Fm. at ~1.8 Ma (G = 15°/Ma).

In the Linxia Basin, the rapid change of stratigraphic dips within a short part of the Wangjiashan section across the Yinchuangou anticline (new data) clearly demonstrates the occurrence of a large set of growth strata that is equivalent to GS1–2 in the nearby Guide Basin. It starts from the uppermost part of the Dongxiang Fm. at ~8 Ma and ends at the truncation of the section at ~1.8 Ma (Fig. 7). Between the Hewangjia Fm. and the Jishi Fm. (boulder conglomerates), a sharp lithological contact (mudstone/boulder conglomerates), a small dip change (~3–5° with a strike change from ~120–125°N to 90°N) above and below the boundary, and detailed paleomagnetic age constraints (the boundary at 4.48–3.6 Ma, ~0.88 Ma of missing strata) all indicate the presence of unconformity U_4 (Li, 1995; Fang and Li, 1998; Li and Fang, 1999; Fang et al., 2003) (Figs. 7a, b).

The other similar sharp lithological contact (alluvial boulder conglomerates/lacustrine siltstone) between the Jishi Fm. and the Dongshan Fm. and detailed paleomagnetic age constraints (~0.1–0.2 Ma strata missing at the boundary) indicate that a pseudo-(parallel) unconformity U_5 exists between the two formations (Li, 1995; Fang and Li, 1998; Li and Fang, 1999; Fang et al., 2003) (Fig. 7a).

The termination of the Dongshan paleolake deposition (the Dongshan Fm.) by the presence of the highest Daxia He and Yellow River terrace gravels (the Jinggoutou Fm.) at ~1.76 Ma indicates the uplift of the basin and draining of the paleo-Dongshan lake, suggesting integration with the Yellow River drainage in the basin (Fig. 7). Especially on the highest terrace, this gravel bed has been subjected to strong folding and erosion to form an evidently eroded (U_6) syncline at the Dongshanding summit, immediately followed by a great incision of the Daxia He and the Yellow River and deposition of loess–paleosol sequences (Figs. 7b, c).

Field investigations have demonstrated that the development of the Yinchuangou anticline, the growth strata and the associated unconformities U_4 to U_6 were all caused by the propagations of faults $F_{5'}$ and $F_{5''}$ rooted from the Leijishan fault F_5, suggesting that the deformation propagated eastwards into the basin at the onset of the strata growth at ~8 Ma (GS1 or U_3) (Figs. 1e and 7).

In the Tianshui Basin, we have not found growth strata in the outcrops, but the deformation can evidently be observed from the presence of unconformities and thrusts folds (Fig. 3). The unconformity U_1 exists between the Palaeogene red fine conglomerate beds and the bedrock below, signifying the onset of the Tianshui Basin. The unconformity U_2 lies between the Neogene red beds and the Palaeogene red fine conglomerate beds or bedrock below.

The high-resolution paleomagnetic dating of the borehole and outcrop sections at Zhuangliang, Qin'an, Yanwan, Yaodian and Lama Shan, constrained by a number of fossil mammals found in the sections and basin (Table 1, Fig. 1f), indicates a southward decrease of the upper age limits of U_2, from ~26 Ma at Zhuanglang at the summit (closest to the Liupan Shan), via Qin'an at ~24.5 Ma and Yanwan at ~17.1 Ma, to Yaodian and Lama Shan at ~12.5 Ma, suggesting southward stepwise down-faulting of the Tianshui Basin (Fig. 3). Unconformity U_3 is marked by the end of the red beds in the most parts of the basin manifesting as a widely distributed erosion surface on the top of the basin, on which only thin Aeolian yellowish loess is superimposed.

Magnetostratigraphy of the measured sections indicates that this erosion surface must have been formed at some time younger than the dated erosion surfaces at ~6.2–5 Ma (Fig. 3). In the southern margin of the basin, U_3 presents either as a pseudo-unconformity in the section or as a minor angular unconformity from the onlap of the red beds onto the Eogene and old bedrock (Li et al., 2006; Wang et al., 2012a,b) (Fig. 3). The southward down-faulting of the Tianshui Basin allowed the Lama Shan section at the southern margin of the basin to have the most complete upper sequence of the basin sediments. Detailed paleomagnetic dating of this section indicates ages of ~3.7–3.4 Ma for U_3, which caused an ~0.3 Ma hiatus of the strata (Fig. 3a). This dating further suggested that unconformity U_4, which is between the Quaternary Aeolian loess and the Neogene lake sediments, might have occurred earliest at the remained erosion surface of the lake sediments of the Lama Shan Fm. at ~2.6 Ma (Wang et al., 2012a,b) (Fig. 3a). During the formation of U_4, the Tianshui Basin was subjected to the strongest thrusting and folding by the North Qin Ling fault, giving rise to the present folds and geomorphology (Maiji Shan upthrusted massif—a famous Buddhist site—the Lama Shan and Tianshui synclines, and the newly down-faulted valley, the Wei He) (Fig. 3). Given that the undeformed highest terrace of the Wei He was paleomagnetically dated to ~1.2 Ma (confirmed by correlation of loess–paleosol sequence and magnetic susceptibility record with their well-dated equivalents on the Chinese Loess Plateau) (Gao et al., 2008; personal communication for more recent progress), the strong tectonic thrusting–folding and rising of the Tianshui Basin must have happened between 2.6 and 1.2 Ma.

https://doi.org/10.1016/j.yqres.2014.01.002 Published online by Cambridge University Press

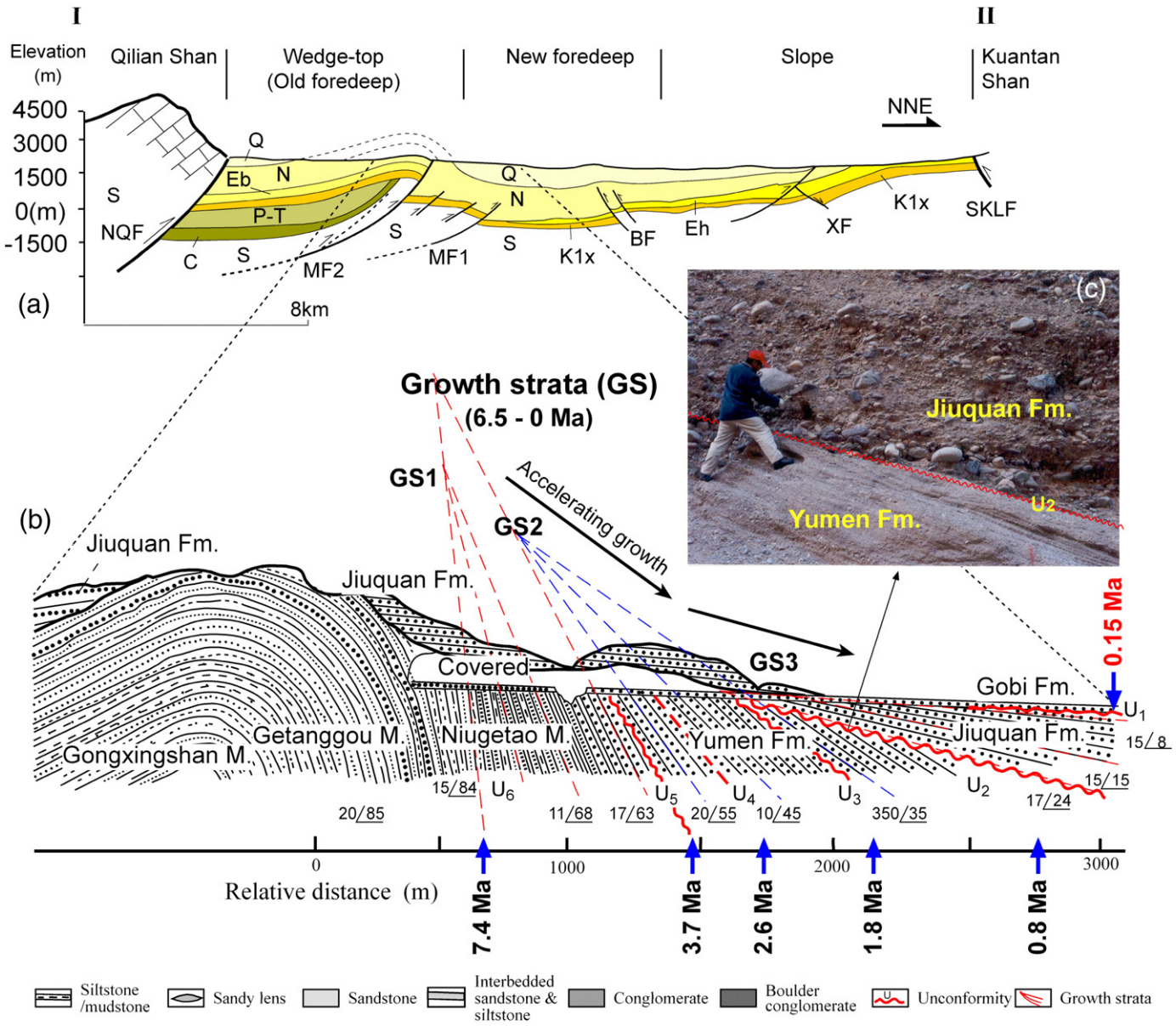

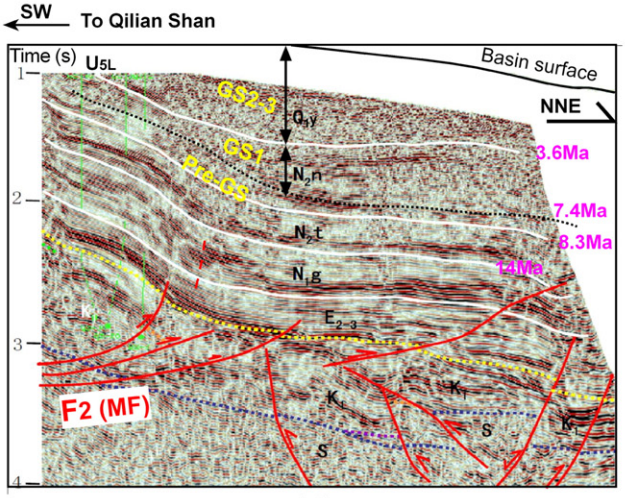

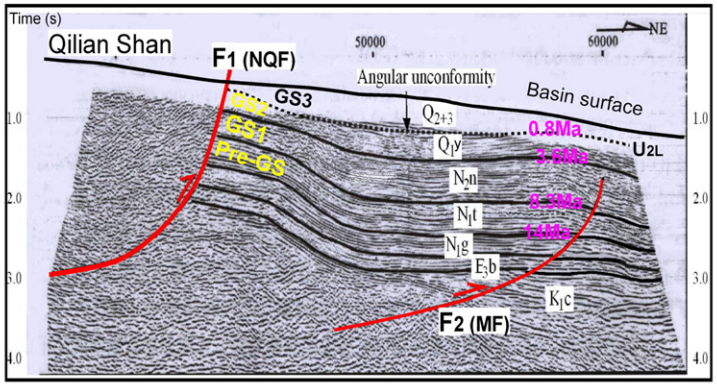

https://doi.org/10.1016/j.yqres.2014.01.002 Published online by Cambridge University Press

In the Liupan Shan, unconformity U_3 lies between the lacustrine–fluvial red beds and the below planation surface, developed on the early Cretaceous rocks in the Shengyu Basin and between the red clay sequence (including some fluvial gravels and sandstone lenses in those near the Liupan Shan) in the Loess Plateau and the underlying planation surface. It demonstrates that the Ordos block and the part of the nearby Liupan Shan massif began to receive sediments at ~8.1 Ma (Fig. 4). This indicates that the Liupan Shan began a rapid uplift and break of the previous planation surface in the Liupan Shan region at ~8.1 Ma (Song et al., 2001). The deposition of the lacustrine–fluvial sediments of the Shengyu Basin was ended by ~3.6 Ma, immediately followed by the Aeolian red clay deposition that was soon terminated at ~3.4 Ma, suggesting that the basin was raised and incorporated into part of the Liupan Shan by the onset of the propagation fault F_3 at ~3.6–3.4 Ma (Fig. 4).

At Shuimo near the Liupan Shan, the red clay sequences were top-eroded and greatly incised by the river to form a clear bedrock-seated terrace. Above the red clay erosion surface (U_5) is an ~50 m loess deposit. Our field investigation of the loess–paleosol sequence and paleomagnetic dating of some key layers confirm that the paleomagnetic Brunhes/Matuyama (B/M) boundary (0.78 Ma) lies in the loess layer L8 (Fig. 4), agreeing well with the nearby Chaona loess magnetostratigraphy results (Song et al., 2000) and all other ones in the Loess Plateau (e.g., Liu, 1985; Ding et al., 1994). This indicates that the river terrace and associated great incision (U_5) occurred at ~0.8 Ma, implying that the Liupan Shan experienced an episodic rapid uplift at that time.

Basin rotation

Basin rotation history provides independent record of tectonic deformation of block and basin. Figure 8 summarises some of our measured sections (Li, 1995; Li et al., 1997a,b, 2006; Song et al., 2000, 2001; Fang et al., 2003, 2005a,b, 2007; Song et al., 2003, 2005; Yan et al., 2006, 2012a; Zhang, 2006; Wang et al., 2012a,b; Zhang et al., 2012, 2013), including unpublished data on the NE Tibetan Plateau. The data demonstrate the following: 1) The whole region within the NE Tibetan Plateau confined by the large envelope boundary faults exhibits an overall pattern of clockwise rotation; 2) The region has been characterised by significant rotations since ~11–8 Ma; and 3) The magnitude of the block clockwise rotations decreases from the west (Qaidam and Guide Basins) at ~25° to the east (Linxia and Tianshui Basins) at ~10° (Fig. 8). All these indicate that the whole NE Tibetan Plateau has been subjected to strong but differential compression and rotations since ~11–8 Ma (Fig. 8).

Other evidence and tectonic deformation and uplift of the NE Tibetan Plateau

Uplift of mountains and propagation of deformation into basins will result in immediate responding changes of lithology, sedimentary facies and rate. Figure 9 summarises the changes of grain size, conglomerate content and sedimentation rate of the studied basins in the NE Tibetan Plateau. The data indicate an overall pattern of rapid increase of the grain size, conglomerate content and sedimentation rate of basin sediments after ~8 ± 1 Ma, and the sedimentation rates accelerated significantly (about doubled) after ~3.6 Ma and again after ~1.8 Ma, even though second-order differences remain among the studied sections and between different time intervals mostly due to the relative distances between the studied sections and the nearby mountains, their locations in thrust–fold belt and basins, and dating uncertainties. In a flexural basin, when thrust–fold belt propagates into the basin, the former parts of the thrust–fold belt will progressively be incorporated into uplifted mountain for erosion as a new detrital source for the basin sediments. In this case, the location of the section to be measured has a great influence on sedimentation rate. Our Wangjiashan section in the Linxia Basin just meets this case where the sedimentation rate shows a persistent decrease since ~8 Ma with faults $F_{5'}$ and $F_{5''}$ propagating into Wangjiashan to raise this place and to form the growth strata (GS1) since that time, whereas the Maogou section located at the front of this newly uplifted thrust–fold belt as a newly created flexural foredeep that has received more sediments, and the sedimentation rate exhibits a significant synchronous long-term increase since ~8 Ma (Figs. 2 and 9h). This also explains why some sections show a decrease of sedimentation rate after ~1.8 Ma (Fig. 9).

Accompanying these increases of the sedimentation rate and conglomerate size and content are changes of sedimentary facies and environments, generally from a low-relief sedimentary facies of lake and distal flood-plain environments, via fan-delta and braided-river settings, to a high-relief sedimentary facies of proximal alluvial fans and debris-flow environments (Figs. 2–4). Figure 10 summarises these lines of tectonic evidence studied in the NE Tibetan Plateau. The data indicate fast shortening and rotating of the studied basins, growing strata and forming multiple regional unconformities, and increases of sedimentation rate, grain size and conglomerate content all began early and synchronously at ~8 ± 1 Ma and accelerated (approximately all doubled or more) after ~3.6 Ma. This is consistent with a general facies change from low- to high-relief environments at 3.6 Ma. All these indicate that significant and repeated uplift of the whole NE Tibetan Plateau began around ~8 ± 1 Ma and increased (approximately doubled in magnitude) after ~3.6 Ma. The results suggest that the present large relief difference between the western and eastern NE Tibetan Plateau was most likely due to differential deformation and uplift of the stronger western and weaker east parts of the NE Tibetan Plateau, rather than the time differences of northeastward growth suggested earlier (e.g., Meyer et al., 1998; Tapponnier et al., 2001). Eastward decreasing of basin rotational magnitudes (~30°–40° in the west; ~20°–15° in the east), strata growth rates (G = ~8–13 cm/ka in the west; 2–6 cm/ka in the east) and sedimentation rates (~30–60 cm/ka in the west; 4–15 cm/ka in the east) after ~8 Ma (Figs. 2–10) corroborate our inference above.

Rock uplift and denudation rates inferred from the low-resolution cooling history of the mountain ranges surrounding the basins in the NE Tibetan Plateau generally indicate a broad rapid cooling and uplift event occurred over the whole NE Tibetan Plateau and the West Qin Ling at ~8 ± 2 Ma (e.g., Molnar, 2005; Enkelmann et al., 2006; Zheng et al., 2006, 2010; Molnar and Stock, 2009; Wang et al., 2012a,b). The work provides a strong support to our inference above.

Origin and development of the Yellow River

The Yellow River (Huang He) originates from the Bayen Kala Shan in the eastern portion of the northern Tibetan Plateau and flows down and cuts northeastwards through the NE Tibetan Plateau (basins and dividing mountains), forming a number of traceable river terraces and gorges. Dating these terraces can indicate when the Yellow River reached the basins through backward incision and how it incised down in response to the episodic stepwise uplifts of the NE Tibetan Plateau as proposed above (Li, 1991; Pan et al., 1991, 2009).

Figure 6. Upper (a): Cross section of I–II in Fig. 1b drawn from seismostratigraphy and field investigations. Middle (b): The measured Laojunmiao outcrop section shows the occurrence of the tectonic events with ages (see heavy arrows) reflected by the developments of the growth strata and unconformities (b, c) (synthesised from Fang et al., 2005a). GPTS: Geomagnetic polarity time scale of Cande and Kent (1995). Bottom (d, e): Seismostratigraphy at the margins of the Jiuquan and Qaidam Basins showing the development of three sets of the growth strata starting at ~8 Ma, 3.6 Ma and 0.8 Ma, respectively. Interpreted stratigraphic boundaries and ages are according to detailed tracing of seismostratigraphy and boreholes with dated cores and outcrop sections partially outlined above. See Fig. 1 for locations.

https://doi.org/10.1016/j.yqres.2014.01.002 Published online by Cambridge University Press

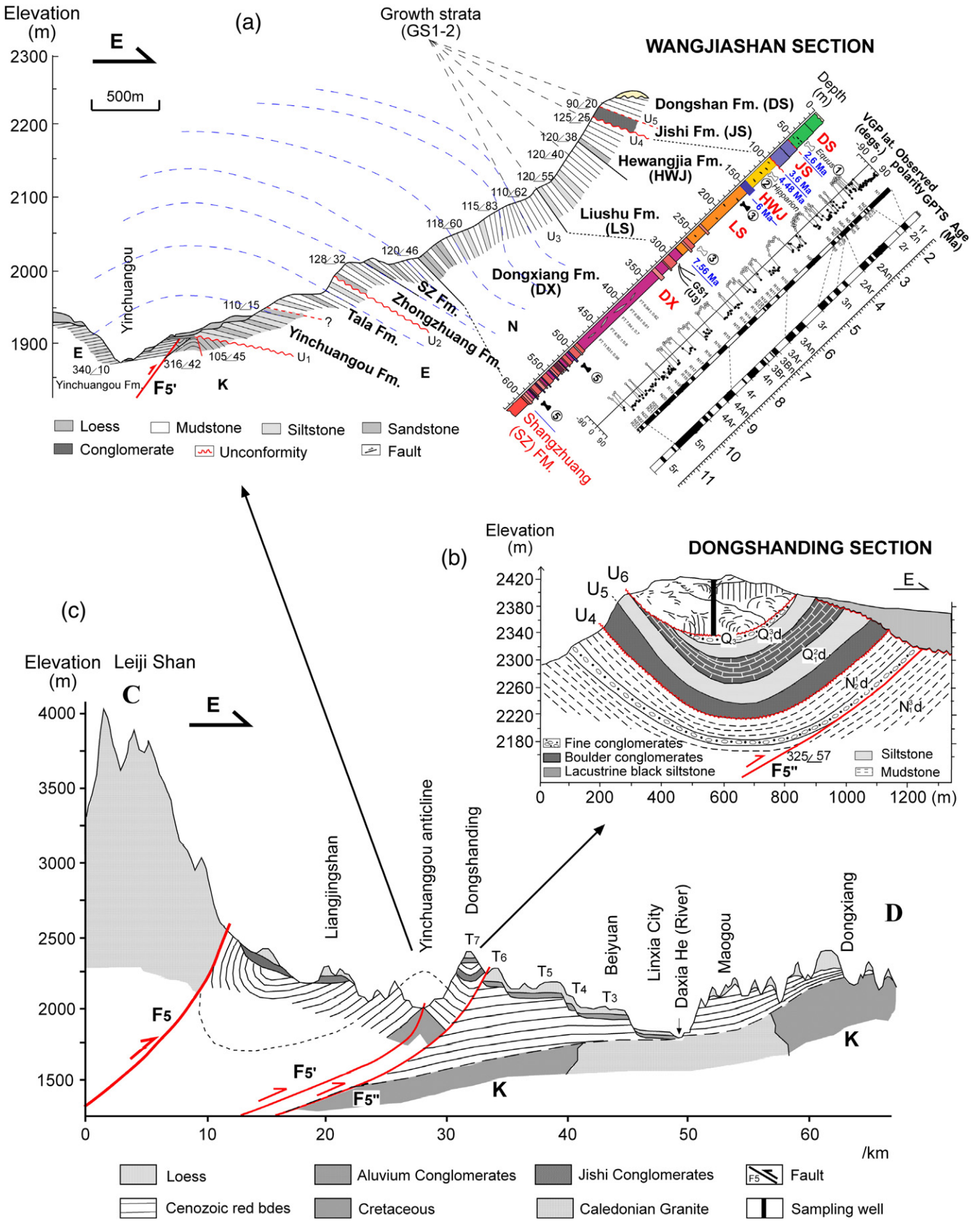

https://doi.org/10.1016/j.yqres.2014.01.002 Published online by Cambridge University Press

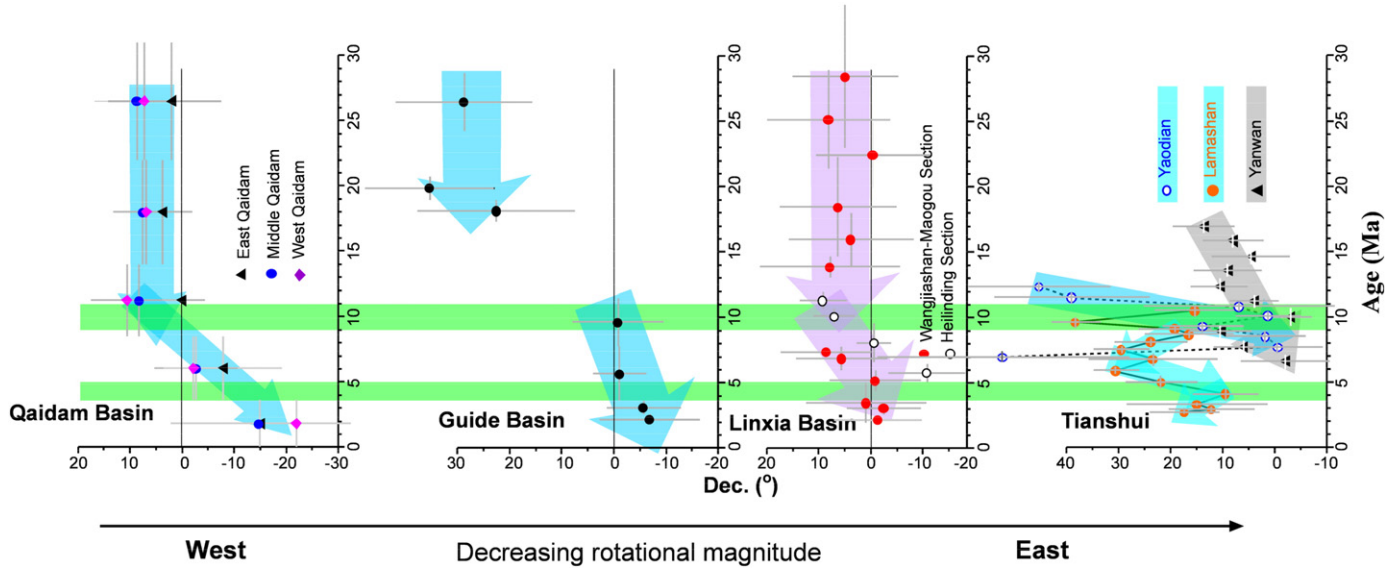

Figure 8. Histories of tectonic rotation of the studied basins on the NE Tibetan Plateau. The error bar in time indicates a time period of stratigraphic intervals averaged. Data with new ones are compiled and recalculated from Li (1995), Li et al. (1997b, 2006), Fang et al. (2003, 2005a,b, 2007), Song et al. (2005), Yan et al. (2006, 2012a), Wang et al. (2012a,b), Zhang et al. (2012) and Zhang et al. (2013).

As most of the river terraces in this region are covered by thick loess, or the basins preserve the youngest lacustrine sediments before the Yellow River appeared in the basins, we can make a detailed chronology of the terraces or basin sediments by applying multiple dating methods (Li, 1991; Pan et al., 1991, 2009; Fang et al., 2005b; Harkins et al., 2007; Craddock et al., 2010; Perrineau et al., 2011). The gravel composition of the highest terrace that can clearly be traced in the present valley of the Yellow River matches that of the modern Yellow River and therefore is regarded as marking the appearance of the present Yellow River. Higher terraces for which angular–subangular gravels have different compositions are regarded as derived from local paleo-rivers within the basins.

Figures 11 and 12 summarise the multi-approach dating of the Yellow River terraces of different basins in the NE Tibetan Plateau and their evolution (e.g., Li, 1991; Pan et al., 1991, 2009; Li, 1995; Li et al., 1996, 1997a; Zhu et al., 1996; Fang et al., 1999; Harkins et al., 2007; Craddock et al., 2010; Perrineau et al., 2011). These works show that the highest terrace gravels of the Yellow River in the large Longzhong Basin (or sub-basins of Jingyuan, Lanzhou and Linxia) (Fig. 1) were all formed immediately after a great incision of the local denudation surface at ~1.8 Ma. Twenty-five pairs of loess–paleosol complexes were formed on this denudation surface and can be dated precisely both by paleomagnetism (the observed normal polarity zone at the bottom of the section was correlated to the top of the Olduvai event) and by correlation of the paleosols with global marine oxygen isotope records (the bottom of loess layer L25 corresponds to isotope stage 62 at ~1.8 Ma) (Li et al., 1996, 1997a; Zhu et al., 1996) (Fig. 11). This suggests that the Longzhong Basin as a whole block experienced the same incision history in response to the uplift of the NE Tibetan Plateau. This is further confirmed by the synchronous development of the subsequent terraces of these three sites (Li, 1991; Pan et al., 1991, 2009; Yue et al., 1991; Li et al., 1996, 1997a) (Figs. 11 and 12).

The start of the highest terrace gravel bed of the Yellow River in the high-elevation Xunhua–Hualong Basin on the Tibetan Plateau was dated to only at ~1.2 Ma, suggesting that the Yellow River extended into the Xunhua–Hualong Basin from the Linxia Basin to the east by retrogressive eroding and carving through the Laji Shan (Jish Gorge) at that time (Li, 1991; Pan et al., 1996) (Figs. 11 and 12).

Farther west in the Gonghe Basin, the deposition of >500 m of fossil-bearing fluviolacustrine Quaternary sediments (Zheng et al., 1985; Xu, 1987) (Table 1) indicates a much later capture of this basin by the Yellow River. When the Yellow River eroded the deep (hundreds of m) Longyang Xia (Gorge) into the Gonghe Basin, ending the basin aggregation and depositing the Yellow River gravels on the basin surface, it was soon followed by stepwise incision of the basin sediments to form a series of terraces. Thick loess or aeolian sand dunes mantle these terraces now. Previous paleontological and paleomagnetic dating of borehole 8105 in the central basin surface, >300 m deep, revealed clear polarity zones that can correlate well to the Brunhes normal and Matuyama reversed chrons and the sub-chrons within them. This indicates that basin sedimentation ended at ~0.12 Ma (Xu, 1987). Organic ^{14}C and OSL dating of the loess sediments on the highest Yellow River terrace places an upper age limit of 30–40 ka for the river incision (Xu, 1987; Li, 1995).

The Gonghe Basin was an area of active sand dunes and dust generation such that any loess deposited was likely reworked down-wind, possibly resulting in hiatuses in loess accumulation during strong wind intervals. The highest Yellow River terrace in the Xinghai–Tongde Basin, a small basin just south of the Gonghe Basin, having a similar surface elevation, and perhaps co-joined in the time of deposition (Fig. 1), was OSL-dated at ~135.7 ± 10.5 ka (Pan et al., 1992). A great incision occurred at ~0.15 Ma after a long period of relatively slow incision in the region (Fig. 11), and the basin drainage with the Yellow River in the Gonghe Basin has been set at ~0.15 Ma (Li, 1991; Li, 1995). This age determination is further supported by recent cosmogenic dating for four Yellow River terraces of 120–250 ka in the Gonghe Basin (Perrineau et al., 2011) and OSL dates averaging 140.7 ± 8.7 ka in the Xinghai–Tongde Basin at (Harkins et al., 2007) (Fig. 12).

Figure 7. Bottom (c): Cross Section C–D in Fig. 1e from the Leiji Shan eastwards to Dongxiang County in the basin centre, showing the intracontinental foreland basin configuration and the thrust–fold belt at wedge-top along the Leiji Shan and its subsequent erosion geomorphology (note the development of the Yellow River and Daxia He terraces T1–T7; see Li et al. (1997a) for detailed age determinations). Middle (b): Enlarged Dongshanding section showing the deformation history revealed occurrences of deformed boulder conglomerate bed, unconformities and highest Yellow River terrace gravel bed. Note two deep wells were dug in the loess covering the highest terrace for sampling and age determination. Top (a): Enlarged part of cross section C–D showing the Yinchuangou anticline and the occurrences of unconformities and two sets of the growth strata (GS1–2) in the Wangjiashan section. The magnetostratigraphy of the section (Li, 1995; Fang et al., 2003) is also plotted on the right for age control. GPTS: Geomagnetic polarity time scale of Cande and Kent (1995).

https://doi.org/10.1016/j.yqres.2014.01.002 Published online by Cambridge University Press

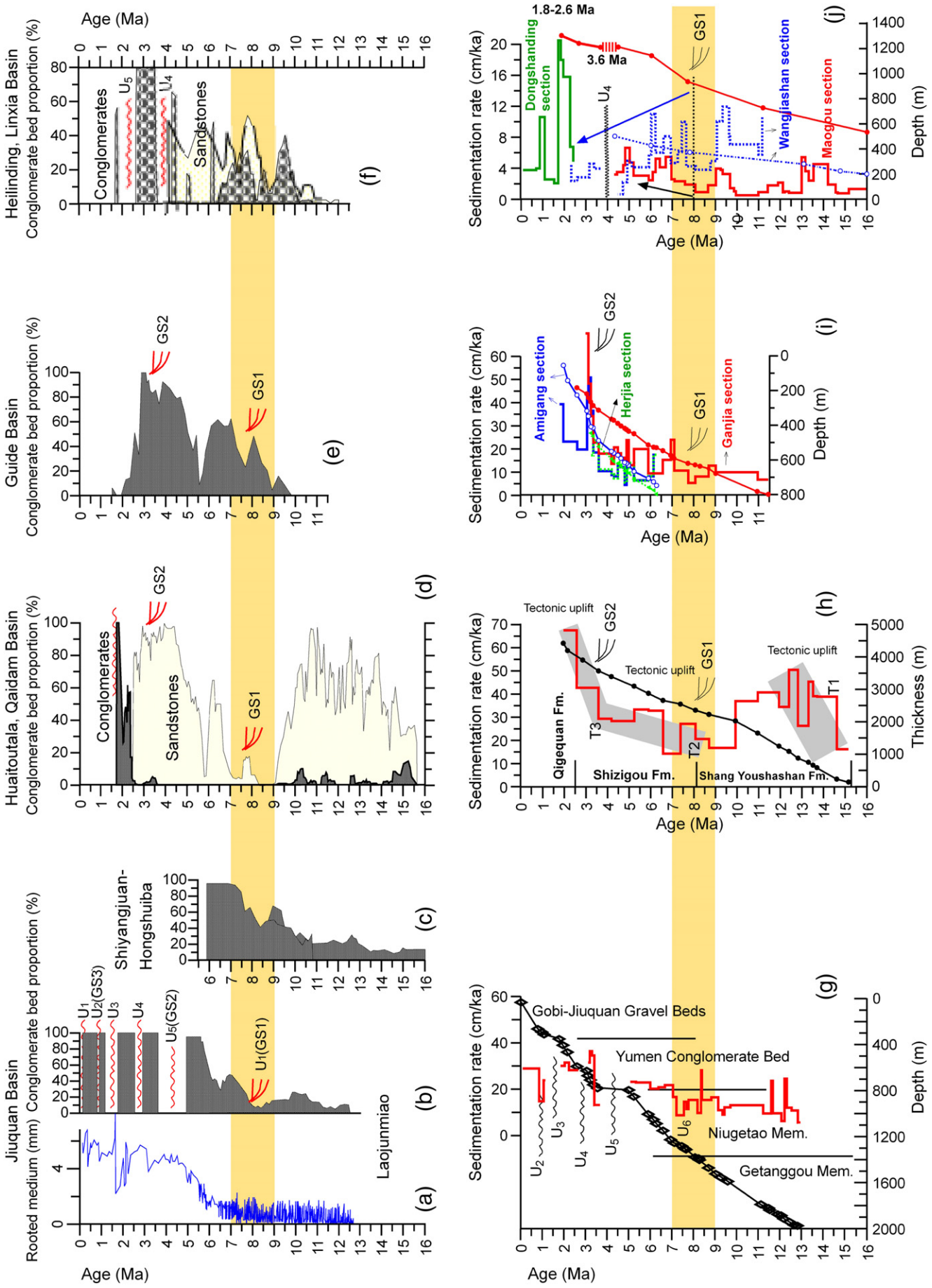

https://doi.org/10.1016/j.yqres.2014.01.002 Published online by Cambridge University Press

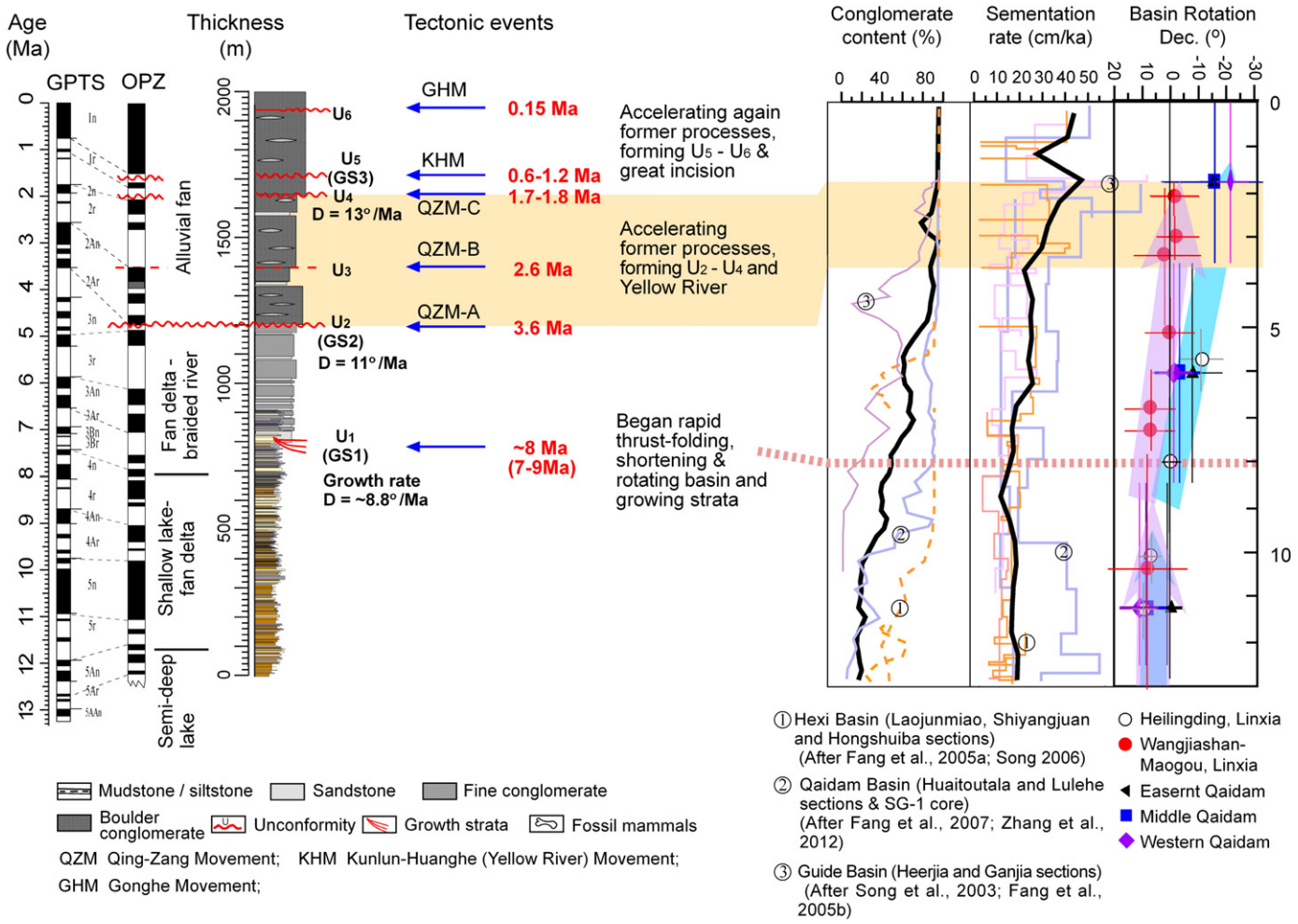

Figure 10. Summary of variations of lithofacies, growth strata, conglomerate content, sedimentation rate and basin rotation on the NE Tibetan Plateau since the late Miocene and their revealed tectonic events and deformation and uplift of the NE Tibetan Plateau. Error bar in the time in rotation indicates a time period of stratigraphic intervals averaged. QZM: Qing–Zang (Tibet) Movement; KHM: Kunlun–Huanghe (Yellow River) Movement; GHM: Gonghe Movement (see Li, 1995; Li et al., 1996 for denominations and details).

Figures 11 and 12 depict the incision history of the Yellow River in the NE Tibetan Plateau and the relationships with the tectonic uplift and climatic change. They demonstrate that there were three rapid incision intervals, at ~1.8–1.4 Ma, ~1.2–0.8 Ma and ~0.15–0.13 Ma, respectively. Only within these intervals did the Yellow River terraces form, irrespective of long-term climate deterioration, and even though each terrace formed at the beginning of each cycle of warm climate when precipitation and hence erosion potential were increased. This timing suggests that tectonic uplift has been the major driver for these rapid incisions (Li, 1991; Pan et al., 2009) (Fig. 11).

These three intervals of rapid incision happened synchronously with the rapid basin deformation at unconformities U_4, U_5 and U_6 in the tectonic viewpoint (meaning large ranges in time and space in recording a tectonic event) (Fig. 10), both indicating rapid episodic uplifts of the NE Tibetan Plateau then. These episodic tectonic uplifts caused the initiation of the Yellow River in the Longzhong Basin (or the sub-basins of Jingyuan, Lanzhou and Linxia) by cutting through the Qingtong Xia (Gorge) at ~1.7 Ma, then headward erosion into the Xunhua Basin at ~1.2 Ma and finally into the Gonghe Basin at ~0.15 Ma (Fig. 12). These episodes were named by Li Jijun as the Qingzang Movement C, the Yellow River Movement and Gonghe Movement, respectively (Li, 1991; Li, 1995; Li and Fang, 1999).

Multi-climatic proxy records and climatic environmental changes

Late Cenozoic deposition in the Linxia Basin was mostly of fine lacustrine fine sediments intercalated with some layers of fluvial sandstones and siltstones at the bottom of each stratigraphic cycle (formation) (Table 1, Fig. 2). Thus, it archives high-quality climatic records. Figure 13 shows sporopollen and anion chlorine records of the Linxia Basin with new anion chlorine data for the early Miocene and late Oligocene (Li, 1995; Fang et al., 1997b; Fang and Li, 1998; Li et al., 1998; Ma et al., 1998). These data demonstrate that the early to middle Miocene forest environment was expressed as dominant warm-temperate broad-leaved trees, and some subtropical trees that were rapidly replaced at ~8–9 Ma by a forest–steppe environment. The transition saw a rapid decrease of trees to <40% and an increase of grasses and shrubs from <25% to >50–70%. Soon after ~5.8 Ma, grasses and shrubs increased to >90%. All these changes indicate fast stepwise drying of the Linxia Basin (Fig. 13).

Figure 9. Variations of grain size (a), occurrences of conglomerate beds calculated for each 50 m stratigraphic interval using 20-m moving-window increments (b–f), sedimentation rates (SR) and depth vs. age plots of the interpreted magnetic polarity chrons (g–j), for the studied sections in different parts of the NE Tibetan Plateau. Note in the Linxia Basin, presented are subsidence curves for the Wangjiashan and Maogou sections (Fang et al., 2003), and the persistent decrease of SR in the Wangjiashan section in the Yinchuangou anticline synchronised the increase of SR in the Maogou section in the basin centre since ~8 Ma, revealing clearly the lifting of the Yinchuangou anticline by propagation faults $F_{5'}$ and $F_{5''}$ and creating a new flexural foredeep further east in the front of the Yinchuangou anticline around the Maogou section (see Fig. 7 for locations and features). U: Unconformity; GS: Growth strata. Compiled with new data from Fang et al. (2003, 2005a,b, 2007).

https://doi.org/10.1016/j.yqres.2014.01.002 Published online by Cambridge University Press

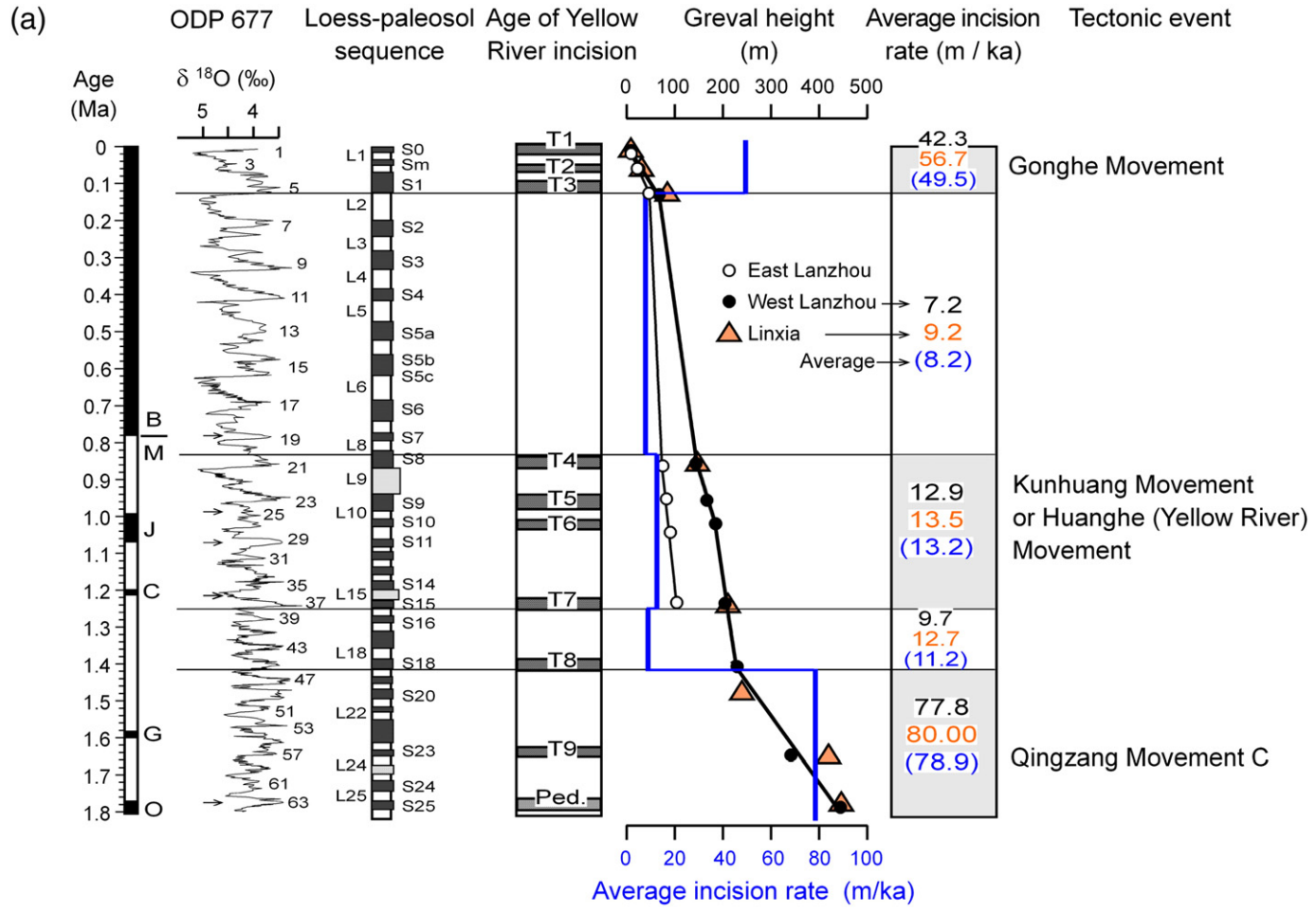

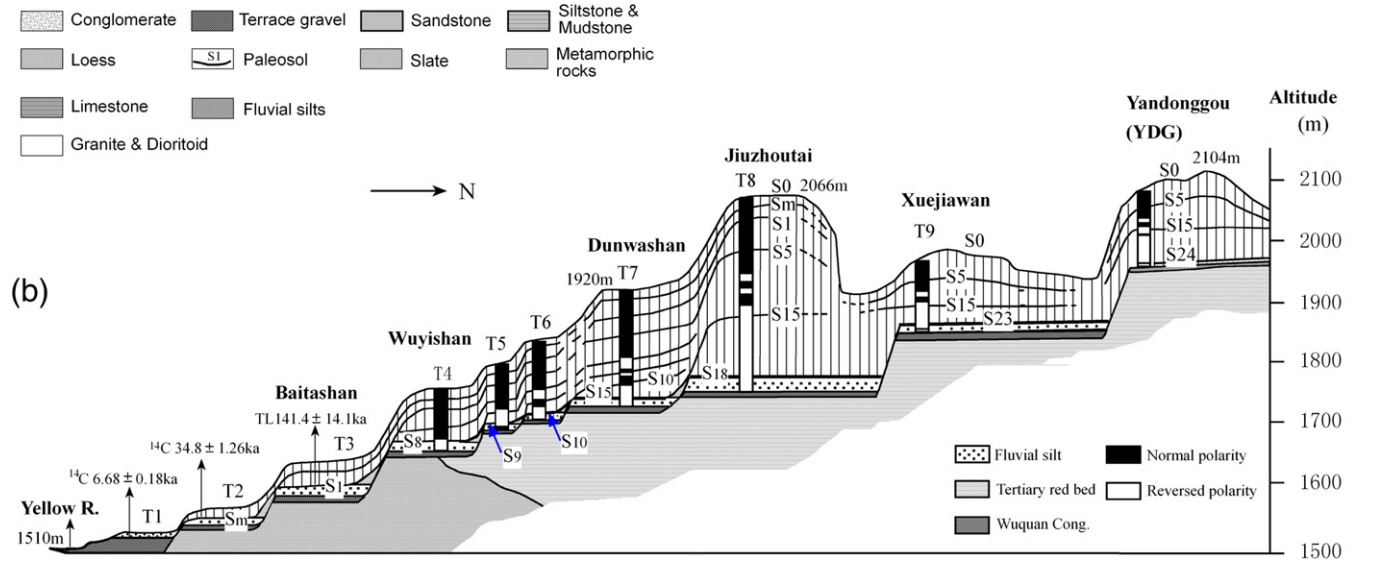

Figure 11. Upper: Correlation of the occurrence and incision of the Yellow River terraces in the Lanzhou and Linxia Basins with the global marine oxygen isotope climate record (Zachos et al., 2008) and the paleosol development in the loess covering the terraces. Bottom: The development of the Yellow River terraces in the Lanzhou Basin. Obtained paleomagnetic stratigraphy and OSL and ^{14}C ages and occurrence of major paleosol layers are shown for terrace age control.
The upper panel is expanded from Pan et al. (2009), with added data from eastern Lanzhou Basin (Chen et al., 1991; Pan et al., 1991) and Linxia Basin (Li et al., 1997a). The bottom panel is modified from Pan et al. (1991), Chen et al. (1991) and Li et al. (1996).

The anion chlorine content, a sensitive index of salinity of lake water, provides a similar climatic record in the Linxia Basin, indicating an increase starting from ~8.5 Ma and accelerating after ~7 Ma and again at ~5.8 Ma (Fang et al., 1997b) (Fig. 13). SEM observations of surface textures of fine-grained quartz and Nd isotope geochemistry of the fine sediments from the Linxia Basin indicate that aeolian dusts were added into the basin during the deposition of lacustrine and fluvial sediments (Wang et al., 1999; Garzione et al., 2005). The increase of

https://doi.org/10.1016/j.yqres.2014.01.002 Published online by Cambridge University Press

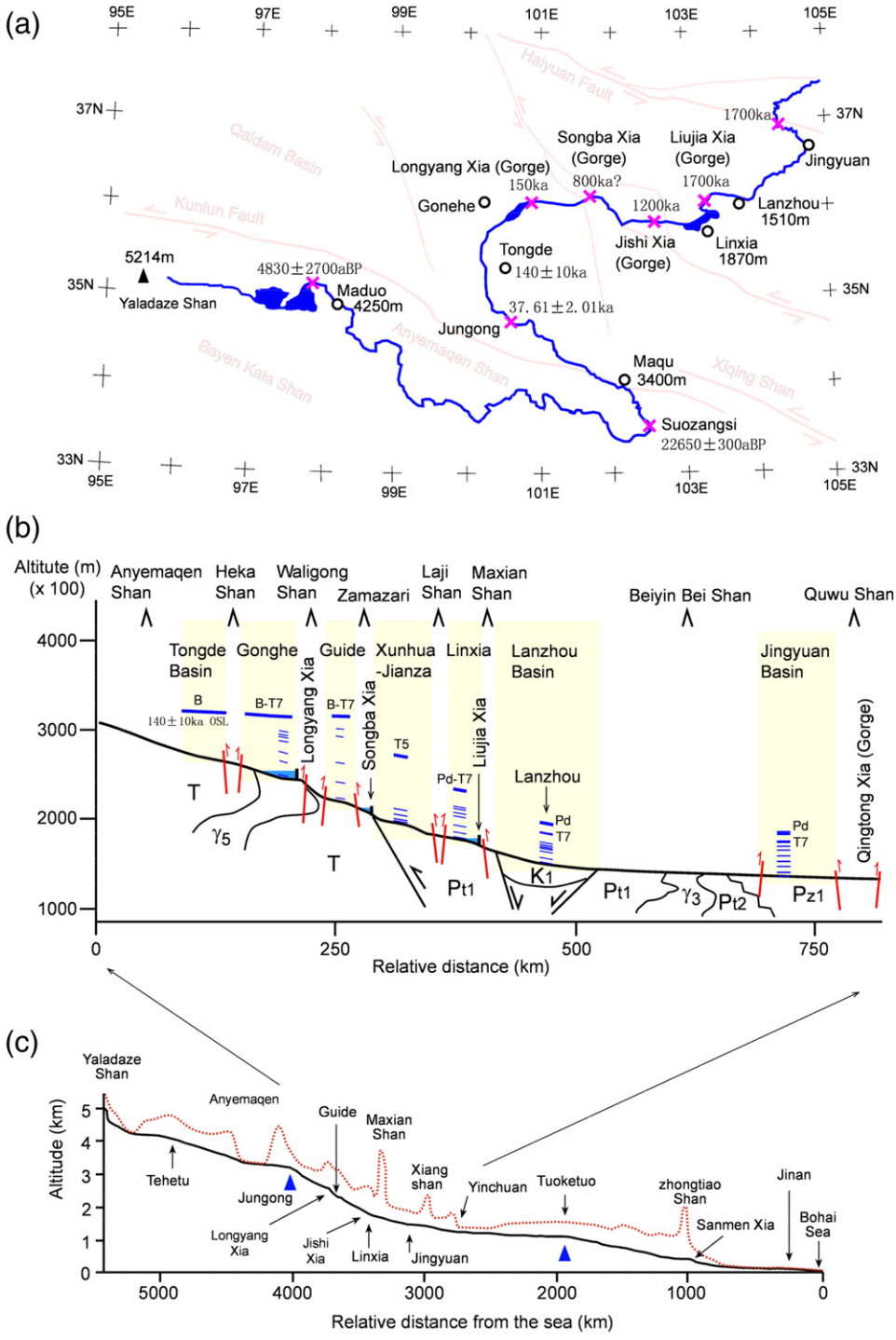

Figure 12. Bottom (c): Yellow River floor and topographic profiles from its head at the summit (Yaladaze Shan) of the Bayen Kala Shan on the Tibetan Plateau to its entry to the Bohai Sea, showing the occurrence of two knick points at Jungong and Tuoketuo indicating large topographic changes from the first topographic step, the Tibetan Plateau to the second topographic step, the Loess Plateau, and then to the third topographic step, the East China Plains. Middle (b): Enlarged part of the Yellow River floor profile between the North Anyemaqen Shan and the Quwu Shan (NW part of the Liupan Shan), showing occurrences of the basin surfaces, pediments and terraces of the Yellow River in the studied basins. Top (a): Diagram showing how the Yellow River was expanded backwards onto the NE Tibetan Plateau by cutting through the gorges between the studied basins. N: Neogene; K1: Lower Cretaceous; T: Triassic; Pz1: Lower Palaeozoic; Pt1: Lower Proterozoic; Pt2: Upper Proterozoic; γ3: Palaeozoic granite; γ5: Mesozoic granite; B: Basin surface; Pd: Pediment surface; T1–T7: Terraces of the Yellow River. Panel a is modified from Li (1991, 1995).

the mass accumulation rate (MAR) of the silt fractions 10–40 mm at ~7.4 and 5.3 Ma in the Linxia Basin have been proven to record the increased Aeolian dust, reflecting a stepwise enhancement of the winter monsoon (dry-cold climate) at those times (Fan et al., 2006).

Figures 14 and 15 from this study summarise representative climatic proxy records from the studied basins in the NE Tibetan Plateau (Fang et al., 1995, 1997b; Li, 1995; Fang and Li, 1998; Li et al., 1998; Ma et al., 1998, 2005a,b; Lü et al., 2001; Wu et al., 2004, 2007, 2011; Bai et al., 2009; Hui et al., 2011; Li et al., 2011; Miao et al., 2011; Cai et al., 2012; Yang et al., 2013). They indicate that profound climatic change occurred at ~8 ± 1 Ma, when long-term aridification began, expressed as a stepwise decrease of trees, an increase of grasses and shrubs (Ma et al., 1998, 2005a,b; Wu et al., 2004, 2007, 2011; Hui et al., 2011; Cai et al., 2012) and an increase of anion chlorine content, a salinity

https://doi.org/10.1016/j.yqres.2014.01.002 Published online by Cambridge University Press

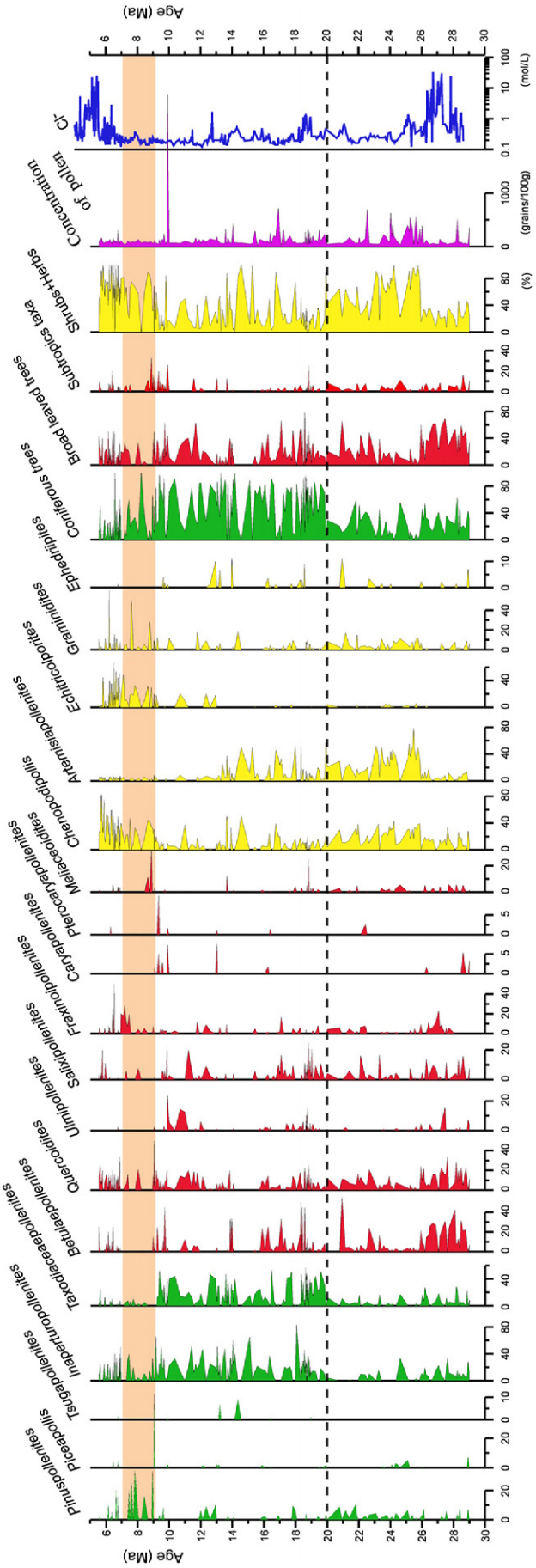

Figure 13. Variations of pollen-spore and anion chlorine records between ~29 Ma and 4.3 Ma in the Linxia Basin. Data from Ma et al. (1998), Fang et al. (1997b), Fang and Li (1998) and Li and Fang (1999).

https://doi.org/10.1016/j.yqres.2014.01.002 Published online by Cambridge University Press

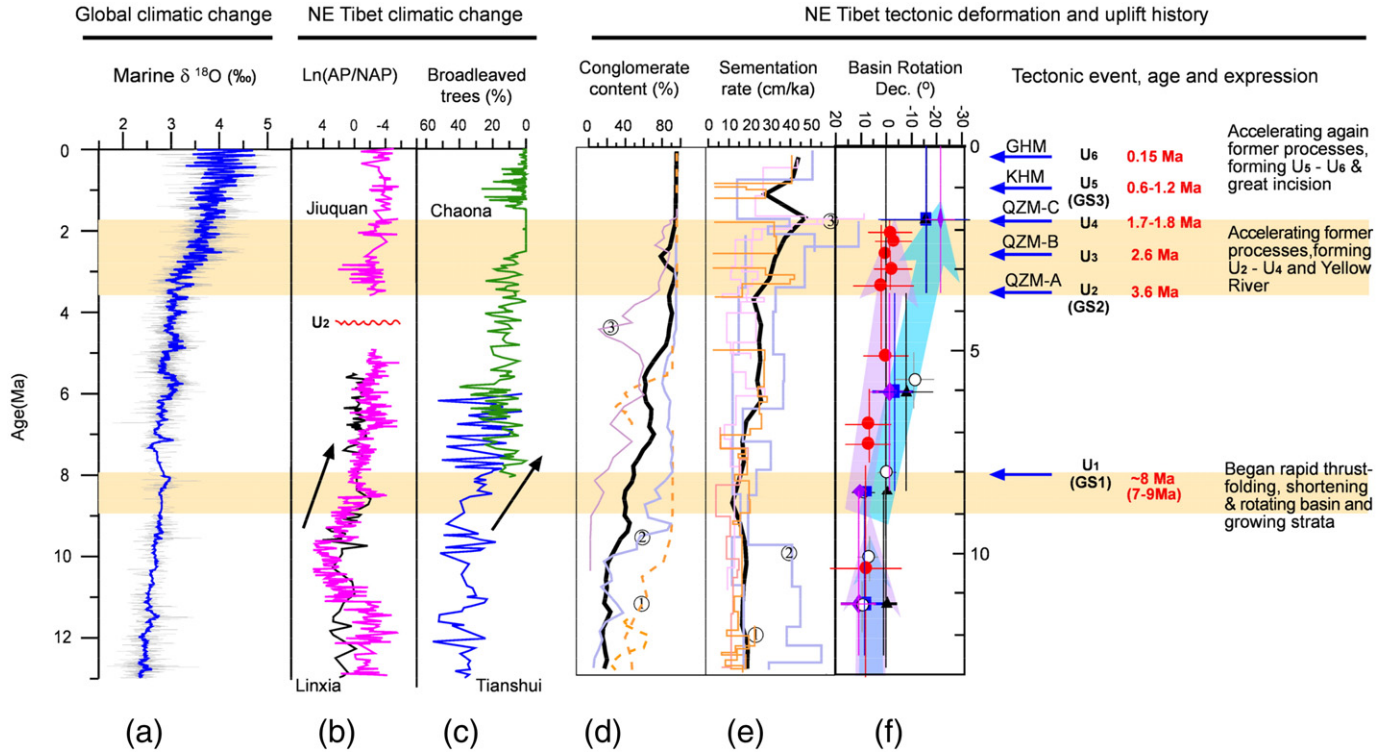

Figure 14. Comparisons of the climatic change with tectonic deformation and uplift history of the NE Tibetan Plateau and global oxygen isotope climatic change (Zachos et al., 2008) since the late Miocene. AP/NAP: Ratio of arbour to non-arbour trees; other legends are the same as Fig. 10.

proxy for water (Li, 1995; Fang et al., 1997b; Li et al., 1998). Subsequent stepwise changes in climate occurred at ~3.6 Ma, 2.6 Ma, 1.8 Ma, 1.2–0.6 Ma and 0.15 Ma, as suggested by pollen records of pollen-spores (Wu et al., 2004, 2007, 2011; Ma et al., 2005a,b; Li et al., 2011; Cai et al., 2012) (Figs. 14, 15a, c) and increased *n*-alkanes C_{31}/C_{27} (representing grasses–shrubs/forests) (Bai et al., 2009) (Fig. 15a), all indicating enhancement of aridification at those times. Furthermore, there is an obvious westward decrease of trees and an increase of herbs and shrubs over the whole studied time interval (~13–0 Ma) in the NE Tibetan Plateau. Between 13 Ma and 8 Ma, trees and herbs–shrubs are ~40–30% and ~50–70% in the Liupan Shan (including nearby Loess Plateau) and Tianshui regions in the east, ~20% and ~40–50% in the Linxia Basin in the middle (Ma et al., 1998), and ~5–10% and ~80–90% in the Jiuquan–Qaidam regions in the west (Ma et al., 2005a; Miao et al., 2011; Wu et al., 2011; Cai et al., 2012), respectively. After ~8 Ma, tree cover was reduced to <10–20% in the east and 2–3% in the west, accompanied with grass and shrub expansion over the whole NE Tibetan Plateau (Figs. 14, 15a). The East Asian monsoon causes eastward moistening of the NE Tibetan Plateau, and the geographic gradients in vegetation suggest that it has existed since ~13 Ma.

Other physical and geochemical proxy records provide robust support for these inferences (Fig. 15). The coarse grain-size fraction (>30 μm) of the Aeolian dust deposits (red clay–loess/paleosol sequence) has been widely used as a sensitive indicator of the intensity of the Asian winter monsoon and its associated dry-cold climate (e.g., Ding et al., 1992; Porter and An, 1995). This proxy record from the Chaona red clay–loess/paleosol sequences to the east of the Liupan Shan (Lü et al., 2001) (Fig. 4) plotted on an astronomically tuned time scale (Han et al., 2011) indicates that persistent increases of grain size started at 3.6 Ma, followed by others at ~2.6 Ma, 1.8 Ma and 1 Ma, all suggesting intensification of the Asian winter monsoon and aridification at those times (Lü et al., 2001; Han et al., 2011) (Fig. 15b). Similar records of grain size increases of dust deposits on the margin of the desert and the Loess Plateau (Ding et al., 2005), the central Loess Plateau (Ding et al., 1994; An et al., 2001) and the North Pacific Ocean (Rea et al., 1998) (Figs. 15f, g, h) also support our inferences.

The high-quality core SG-1, nearly 1000 m long, from the centre of the western Qaidam Basin, because of its continuity, high sedimentation rate and fine sediments formed in a closed lake, has been proven thus far to be the best record of the Plio-Quaternary climatic change during ~2.8–0.1 Ma in the Asian inland region (Wang et al., 2012a,b; Zhang et al., 2012). The Mn concentration in acetic acid leaching (Mn_{HOAc}) is mostly responsible for bivalent Mn^{++} fluctuations in carbonate phases and thus has been proposed as a new sensitive indicator of paleolake redox evolution and catchment-scale climate change (Yang et al., 2013) (Fig. 15d). The Mn_{HOAc} variation in core SG-1 provides further support and indicates a long-term upward decreasing trend marked by several stepwise rapid drops at ~2.5 Ma, 1.8 Ma, 1.2 Ma and 0.6 Ma. These indicate a long-term stepwise decrease of reactive Mn input from catchment weathering associated with increasing oxygen content in the paleolake bottom water. This suggests a long-term stepwise drying of the Asian inland at those times (Yang et al., 2013) (Fig. 15d).

Fossils found in the Huaitoutala section and other nearby sections in the Qaidam Basin show that many large mammals such as rhinoceroses, elephants and giraffes lived there in the late Miocene and early Pliocene but disappeared in the Quaternary. Given that these mammals require grasses for food, their presence suggests that the climate in the late Miocene and early Pliocene was much warmer and moister than during the Quaternary, including the present time (Wang et al., 2007; Zhang et al., 2012). Diets revealed by enamel tooth carbon and oxygen isotopes confirmed this, indicating a drying trend of the climate in the Qaidam Basin (Zhang et al., 2012).

The content of broadleaved trees in pollen-spore records in the NE Tibetan Plateau at 13–6 Ma decreases westwards from 30.6% in Tianshui Basin, to 20.3% in the Linxia Basin, and 5.0% in the Jiuquan Basin (the figure is not presented here), indicating that moisture gradient similar to the modern one, with a drier west and relatively moister east, already existed in the late Miocene.

https://doi.org/10.1016/j.yqres.2014.01.002 Published online by Cambridge University Press

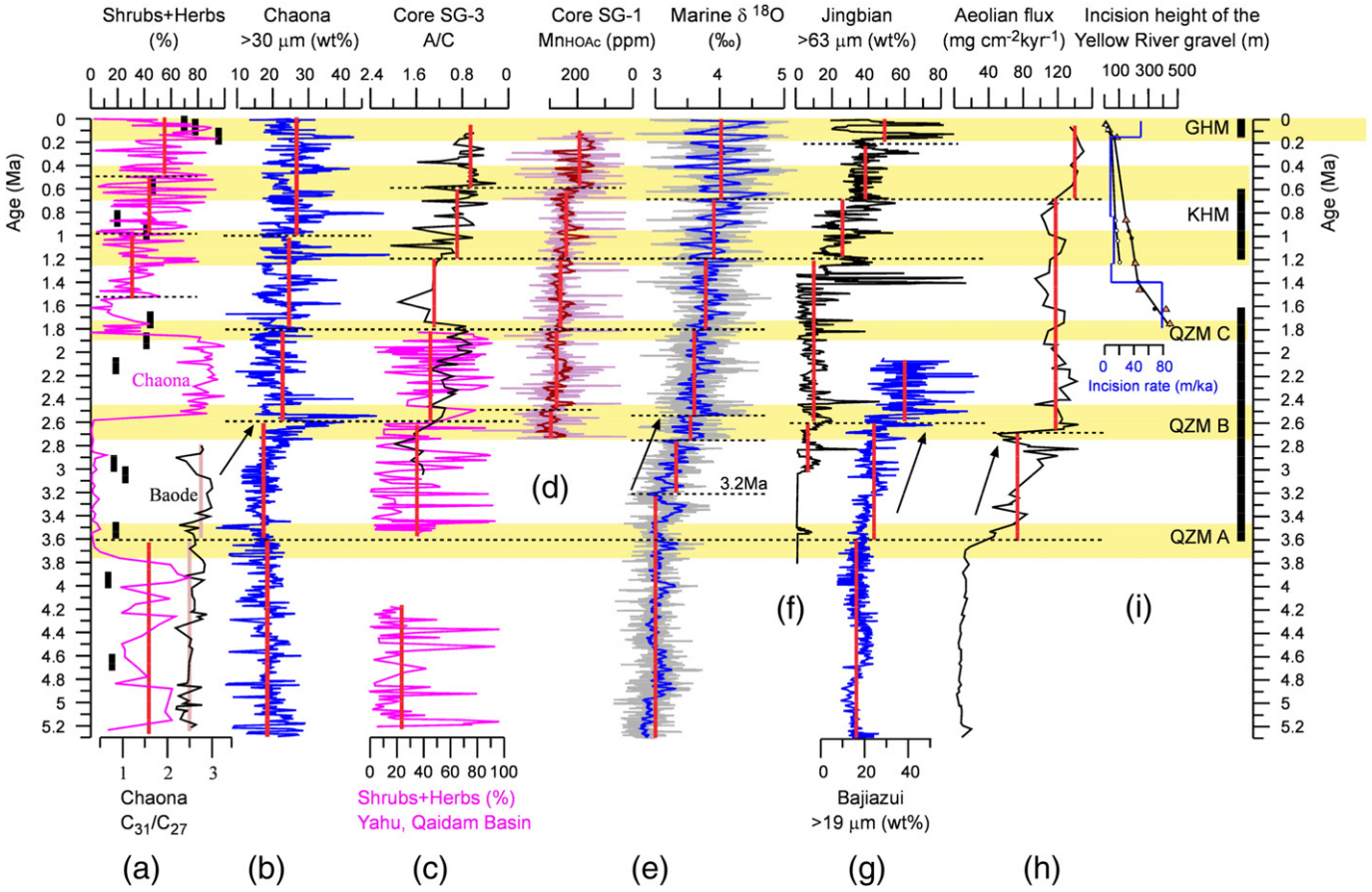

Figure 15. Comparisons of the climatic records from the Chaona section on the Loess Plateau and the Qaidam Basin on the NE Tibetan Plateau with the incision history of the Yellow River and the global oxygen isotope climatic change (Zachos et al., 2008) since the Pliocene. Legends are same as Fig. 10.
For the Chaona section, the sporopollen records are compiled from Wu et al. (2004), Ma et al. (2005b) and Li et al. (2011); the organic biomarker record is from Bai et al. (2009); and the grain-size record is from Lü et al. (2001). For the Qaidam Basin, the sporopollen records were compiled from Wu et al. (2007) and Cai et al. (2012); and the MnHOAc records of the core SG-1 are from Yang et al. (2013). Grain size records from other sections on the Loess Plateau (the Bajiazui section from An et al., 2001; the Jingbian section (Ding et al., 2002) and North Pacific Ocean (Rea et al., 1998) are also plotted for comparison.

Interaction of tectonic uplift of the NE Tibetan Plateau and climatic change

Comparisons of the late Miocene–Quaternary climatic change of the NE Tibetan Plateau with its tectonic deformation and uplift history and the global climatic change demonstrate a generally good match of the drying of the Asian inland and intensification of the Asian winter monsoon or weakening of the Asian summer monsoon with the deformation and uplift history of the NE Tibetan Plateau. For example, the persistent profound drying of the Asian inland and NE Tibetan Plateau and weakening of the Asian summer monsoon after ~8–9 Ma match the beginning of the pervasive rapid deformation and uplift of the NE Tibetan Plateau at that time. Further stepwise rapid drying of the region and enhancements of the Asian winter monsoon at ~3.6 Ma, 2.6 Ma, 1.8 Ma, 1.2–1 Ma, 0.6 Ma and 0.15 Ma match the episodes of accelerated deformation and uplift of the NE Tibetan Plateau at those same times, such as the three episodes of the Qing–Zang Movement (QZM A, B, C), the Kunlun–Huanghe (Yellow River) Movement (KHM) and the Gonghe Movement (GHM) (Figs. 14 and 15). We observed that before ~3.2 Ma, there was no significant agreement between the drying of Asia and the global climatic change, but after ~3.2 Ma, a general match of the Asian drying and the global climatic cooling becomes evident (Fig. 15), suggesting that the global cooling likely contributed to drying at those times.

We believe that within error ranges, the good match of tectonic deformation and uplift of the NE Tibetan Plateau with climatic changes (drying) both in long-term trend and episodes is significant. We know that there are a number of ways to introduce uncertainties into the determination of tectonic and climatic events. The first is the resolution and completeness of the paleomagnetic data from the studied basins. Because we obtained high quality and resolution of magnetostratigraphies (nearly all polarity chrons in the GPTS can be observed; see Fig. 2) by carefully selecting representative sections from the studied basins that were as long and as continuous as possible, and with as fine sediments as possible, and by sampling at dense and nearly equal intervals (~0.5–1 m for fine sediments and ~1–3 m for conglomerates), and because we used many fossil mammals found in the measured sections or equivalent stratigraphic beds in the studied basins together with other numerical dating methods (organic ^{14}C, TL/OSL, ESR and U/Th) to help constrain the stratigraphy, our correlations of the obtained polarity zones with the GPTS are very successful and constrain errors mostly within several to tens of thousands of years (see Fig. 2 and those in related references for details).

The second source of uncertainty comes from the fact that the different lines of evidence we obtained from different methods or proxy records having various resolutions and sensitivities show different uncertainties. For example, rotation data are averaged from large stratigraphic intervals (usually based on one or several formation units) covering millions of years, whereas pollen, gravel-content and size records have much finer resolutions (several tens of thousands of years) than other easily measured proxy records. The strength of tectonism and the locations of the studied sections in thrust–fold belts and basins greatly affect the sensitivities of some proxies recording deformation and uplift, sedimentation rate and grain size. Nevertheless, we

https://doi.org/10.1016/j.yqres.2014.01.002 Published online by Cambridge University Press

found obvious uncertainties from different lines of evidence or records only of ±1 Ma for the 8 Ma tectonic event. The uncertainties for other events are mostly around several tens of thousands to one hundred years. In terms of long-term records and tectonic viewpoints, such uncertainty scales can be ignored.

Two other lines of arguments lend further support to the correlations discussed above. In the temporal domain, the synthesised records all show a long-term drying of the NE Tibetan Plateau since the late Miocene. This should lead to a long-term reduction of erosion power in the region, giving rise to long-term decreases of sedimentary delivery and grain size and weakening of denudation-related rebound uplift of the ranges. Obviously, this is contradicted by the proxy records and the enhanced tectonic uplift since the late Miocene (Figs. 8–10, 14, 15). In the spatial domain, from the east to west of the NE Tibetan Plateau, the tectonic deformation and uplift intensified while the climate became more arid, demonstrating again a contradiction between the topography and tectonism and climate (erosion power). For example, in the west, high topography and stronger tectonism is associated with drier climate and weakened erosion power, whereas in the east it is the opposite. Therefore, we believe that the good correlation between tectonic and climatic events above implies that the entire but differential tectonic uplift of the NE Tibetan Plateau may be the major force that has been driving the climatic "deterioration" in the region.

Several mechanisms have long been thought to contribute to the drying of the Asian interior. Uplift of the Tibetan Plateau is one of the widely accepted mechanisms. First, the uplifted Tibetan Plateau can hinder moisture input from the Indian and East Asian monsoons. Second, the raised plateau will hinder, deflect and enhance the westerlies, resulting in sinking dry flows of air in large areas in central Asia and the eastern Mediterranean (Ruddiman and Kutzbach, 1989). Third, the raised plateau may cause global cooling, thus leading to a reduced evaporation of global surface waters and the drying of continental interiors (Ruddiman and Kutzbach, 1989; Broccoli and Manabe, 1992). The retreat of the Para-Tethys Sea may also have brought about the aridification of the Asian interior (Ramstein et al., 1997). However, the retreat is also widely thought to have been caused also by the uplift of the Tibetan Plateau (e.g., Bosboom et al., 2011).

Geologic evidence and GCM modelling have demonstrated that uplift of the Tibetan Plateau can intensify the Asian monsoon and aridification of the Asian interior (Kutzbach et al., 1989, 1993; Ruddiman and Kutzbach, 1989; Manabe and Broccoli, 1990; Broccoli and Manabe, 1992; Molnar et al., 2010). Using detailed modelling of climates in response to differential uplift of the Tibetan Plateau in much higher time and space resolutions, Liu and Yin (2002) demonstrated that uplift of the NE Tibetan Plateau plays a fundamental role in enhancing the East Asian monsoon and in drying the interior, but plays only a minor role in the Indian monsoon, whereas uplift of the southern Tibetan Plateau and Himalaya has a great impact on enhancing the Indian monsoon but only a minor one on the East Asian monsoon. Using atmosphere–ocean coupled GCM modelling, Abe et al. (2003) further indicated that uplift of the NE Tibetan Plateau has much larger influence on the East Asian monsoon through the amplifying effect (feedbacks) of atmosphere–ocean coupled system. All these modelling experiments agree well with our detected coupling of uplift of the NE Tibetan Plateau and drying of the Asian inland and enhancing of the East Asian winter monsoon (or weakening of the East Asian summer monsoon) (Figs. 14 and 15), thus providing robust support to our inferences that persistent stepwise accelerated uplifts of the NE Tibetan Plateau have driven the persistent stepwise accelerated aridification of the Asian inland and NW China since ~8 Ma, and the global cooling may have added its contributions since ~3.2 Ma.

Conclusions

1) Paleomagnetic, OSL and ^{14}C dating of the late Cenozoic basin and river-terrace sediments in parts of the NE Tibetan Plateau have established high-resolution stratigraphic chronologies for the late Miocene–Quaternary.
2) Field investigations and seismo-stratigraphic analyses of thrust–fold belts along the basin margins revealed that three sets of growth strata and six unconformities were developed in the late Miocene to Quaternary stratigraphy with ages ~8 ± 1 Ma, 3.6 Ma, 2.6 Ma, 1.8–1.7 Ma, 1.2–0.6 Ma and 0.15 Ma, respectively, suggesting that the deformation rapidly propagated through the basins at those times.
3) Paleomagnetic declinations indicate an overall pattern of clockwise rotation within the NE Tibetan Plateau, commencing rapidly after ~11–8 Ma, with rotational magnitudes decreasing eastwards.
4) The variations of grain size, conglomerate content and sedimentation rate of basin sediments in the NE Tibetan Plateau indicate an overall pattern of rapid increase of these parameters since ~8 ± 1 Ma, especially for sedimentation rates which nearly doubled after ~3.6 Ma. Sedimentary facies and the environment mostly changed from low-relief sedimentary facies associated with lake and distal flood-plain environments, via fan deltas and braided rivers, to high-relief sedimentary facies associated with proximal alluvial fans and debris flows.
5) The detailed dating of the Yellow River terraces in the NE Tibetan Plateau shows that the Yellow River there initiated in the large Longzhong Basin at ~1.7 Ma and episodically stepped onto the topographic Tibetan Plateau by backward erosion at ~1.2 Ma, 0.8 Ma and 0.15 Ma in response to the stepwise uplifts of the NE Tibetan Plateau at those times.
6) High-resolution multi-climatic proxy records from the basins and terrace sediments in the NE Tibetan Plateau demonstrate that a persistent enhancement of the East Asian winter monsoon (EAWM) and drying of the Asian interior began at ~8 ± 1 Ma. This phenomenon was expressed as a transition from dominant forest environments to dominant steppe environments and was followed by further winter monsoon enhancements and dryings at ~3.6 Ma, 2.6 Ma, 1.8 Ma, 1.2–0.6 Ma and 0.15 Ma,
7) The tectonic and sedimentary evidence demonstrated that the rapid persistent rise of the NE Tibetan Plateau began ~8 ± 1 Ma and was followed stepwise by accelerated rises at ~3.6 Ma, 2.6 Ma, 1.8–1.7 Ma, 1.2–0.6 Ma and 0.15 Ma, coinciding with the long-term but stepwise drying of the Asian interior at those times. The uplift events were coupled with global cooling events after ~3.2 Ma. This suggests that the tectonic uplift of the NE Tibetan Plateau has been the major forcing factor driving the enhancements of the EAWM and aridification, although global cooling has exerted some control since ~3.2 Ma.

Acknowledgments

This study was supported by the (973) National Basic Research Program of China (2013CB956400, 2011CB403000), the Strategic Priority Research Program of the Chinese Academy of Sciences (Grant No. XDB03020400) and NSFC grants (41321061, 40920114001). Many thanks are given to Drs. Zhang Weilin, Meng Qingquan, Wu Fuli and Han Wenxia for their assistance in calculating data and drawing diagrams.

References

Abe, M., Kitoh, A., Yasunari, T., 2003. An evolution of the Asian summer monsoon associated with mountain uplift—simulation with the MRI atmosphere–ocean coupled GCM. Journal of the Meteorological Society of Japan 81, 909–933.

An, Z.S., Kutzbach, J.E., Prell, W.L., Porter, S.C., 2001. Evolution of Asian monsoons and phased uplift of the Himalaya–Tibetan plateau since Late Miocene times. Nature 411, 62–66.

Bai, Y., Fang, X.M., Nie, J.S., Wang, Y.L., Wu, F.L., 2009. A preliminary reconstruction of the paleoecological and paleoclimatic history of the Chinese Loess Plateau from the application of biomarkers. Palaeogeography Palaeoclimatology Palaeoecology 271, 161–169.

Bosboom, R.E., Dupont-Nivet, G., Houben, A.J.P., Brinkhuis, H., Villa, G., Mandic, O., Stoica, M., Zachariasse, W.J., Guo, Z., Li, C., Krijgsman, W., 2011. Late Eocene sea retreat from the Tarim Basin (west China) and concomitant Asian paleoenvironmental change. Palaeogeography Palaeoclimatology Palaeoecology 299, 385–398.

https://doi.org/10.1016/j.yqres.2014.01.002 Published online by Cambridge University Press

Broccoli, A.J., Manabe, S., 1992. The effects of orography on midlatitude northern hemisphere dry climates. Journal of Climate 5, 1181–1201.
Burbank, D.W., Li, J.J., 1985. The age and paleoclimatic implications of the loess of Lanzhou, north China. Nature 316, 429–431.
Burchfiel, B.C., Deng, Q.D., Molnar, P., Royden, L., Wang, Y.P., Zhang, P.Z., 1989. Intracrustal detachment with zones of continental deformation. Geology 17, 448–452.
Cai, M.T., Fang, X.M., Wu, F.L., Miao, Y.F., Appel, E., 2012. Pliocene–Pleistocene stepwise drying of Central Asia: evidence from paleomagnetism and sporopollen record of the deep borehole SG-3 in the western Qaidam Basin, NE Tibetan Plateau. Global and Planetary Change 94–95, 72–81.
Cande, S.C., Kent, D.V., 1995. Revised calibration of the geomagnetic polarity timescale for the Late Cretaceous and Cenozoic. Journal of Geophysical Research 100, 6093–6095.
Chen, F.H., Li, J.J., Zhang, W.X., 1991. Loess stratigraphy of the Lanzhou profile and its comparison with deep-sea sediment and ice core record. GeoJournal 24, 201–209.
Clark, M.K., Farley, K.A., Zheng, D.W., Wang, Z.C., Duvall, A.R., 2010. Early Cenozoic faulting of the northern Tibetan Plateau margin from apatite (U–Th)/He ages. Earth and Planetary Science Letters 296, 78–88.
Craddock, W.H., Eric Kirby, N.W., Harkins, H., Zhang, X.S., Liu, J.H., 2010. Rapid fluvial incision along the Yellow River during headward basin integration. Nature Geoscience. http://dx.doi.org/10.1038/NGEO777.
Dai, S., Fang, X.M., Song, C.H., Gao, J.P., Gao, D.L., Li, j.j, 2005. Early tectonic uplift of the northern Tibetan Plateau. Chinese Science Bulletin 50, 1642–1652.
Ding, Z.L., Rutter, N.W., Han, J.T., Liu, T.S., 1992. A coupled environmental system formed at about 2.5 Ma over eastern Asia. Palaeogeography Palaeoclimatology Palaeoecology 94, 223–242.
Ding, Z.L., Yu, Z.W., Rutter, N.W., Liu, T.S., 1994. Towards an orbital time scale for Chinese loess deposits. Quaternary Science Reviews 13, 39–70.
Ding, Z.L., Derbyshire, E., Yang, S.L., Yu, Z.W., Xiong, S.F., Liu, T.S., 2002. Stacked 2.6 Ma grain size record from the Chinese loess based on five sections and correlation with the deep-sea $\delta^{18}O$ record. Paleoceanography 17, 5-1–5-21.
Ding, Z.L., Derbyshire, E., Yang, S.L., Sun, J.M., Liu, T.S., 2005. Stepwise expansion of desert environment across northern China in the past 3.5 Ma and implications for monsoon evolution. Earth and Planetary Science Letters 237, 45–55.
Dupont-Nivet, G., Krijgsman, W., Langereis, C.G., Abels, H.A., Dai, S., Fang, X.M., 2007. Tibetan plateau aridification linked to global cooling at the Eocene–Oligocene transition. Nature 445, 635–638.
England, P.C., Houseman, G.A., 1989. Extension uring continental convergence, with application to the Tibetan Plateau. Journal of Geophysical Research 94, 17,561–17,579.
Enkelmann, E., Ratschbacher, L., Jonckheere, R., Nestler, R., Fleischer, M., Gloaguen, R., Kacker, B.R., Zhang, Y.Q., Ma, Y.S., 2006. Cenozoic exhumation and deformation of northeastern Tibet and the Qinling: is Tibetan lower crustal flow diverging around the Sichuan Basin? Geological Society of America Bulletin 118, 651–671. http://dx.doi.org/10.1130/B25805.1.
Fan, M.J., Song, C.H., Dettman, D.L., Fang, X.M., Xu, X.H., 2006. Intensification of the Asian winter monsoon after 7.4 Ma: grain-size evidence from the Linxia Basin, northeastern Tibetan Plateau, 13.1 Ma to 4.3 Ma. Earth and Planetary Science Letters 248, 171–182.
Fang, X.M., Li, J.J., 1998. Late Cenozoic uplift of the Tibetan Plateau and environmental change. (in Chinese) In: Shi, Y.F., Li, J.J., Li, B.Y. (Eds.), Late Cenozoic Uplift of the Qinghai–Tibetan Plateau and Environmental Changes. Guangdong Science and Technology Press, Guangzhou, pp. 394–414.
Fang, X.M., Li, J.J., Zhu, J.J., Zhong, W., Wang, J.L., Lu, W.Q., Hao, Y.P., Gao, J.X., Cheng, H.L., Kang, S.C., Wang, J.M., Zhang, Y.C., 1995. A 30 million-year record of the carbonate content of the Linxia Basin and its climatic implications. (in Chinese with English abstract) In: Tibetan Project Expert Commission (Ed.), Studies on Formation and Evolution of the Tibetan Plateau, Environmental Changes and Ecological System, Paper Collections (1994). Science Press, Beijing, pp. 55–65.
Fang, X.M., Li, J.J., Zhu, J.J., Chen, H.L., Cao, J.X., 1997a. Absolute age determination and division of Cenozoic stratigraphy in the Linxia Basin of Gansu Province, China. Chinese Science Bulletin 42, 1457–1471 (in Chinese).
Fang, X.M., Xi, X.X., Li, J.J., Mu, D.F., 1997b. Late Miocene drying of Western China. Chinese Science Bulletin 42, 2521–2524 (in Chinese).
Fang, X.M., Pan, B.T., Guan, D.H., Li, J.J., Ono, Y., Fukusawa, H., Oi, K., 1999. A 60,000-year loess–paleosol record of millennial-scale summer monsoon instability from Lanzhou, China. Chinese Science Bulletin 44, 2264–2267.
Fang, X.M., Garzione, C., Van der Voo, R., Li, J.J., Fan, M.J., 2003. Flexural subsidence by 29 Ma on the NE edge of Tibet from the magnetostratigraphy of Linxia Basin, China. Earth and Planetary Science Letters 210, 545–560.
Fang, X.M., Yan, M.D., Van der Voo, R., Rea, D.K., Song, C.H., Parés, J.M., Gao, J.P., Nie, J.S., Dai, S., 2005a. Late Cenozoic deformation and uplift of the NE Tibetan Plateau: evidence from high-resolution magnetostratigraphy of the Guide Basin, Qinghai Province, China. Geological Society of America Bulletin 117, 1208–1225.
Fang, X.M., Zhao, Z.J., Li, J.J., Yan, M.D., Pan, B.T., Song, C.H., Dai, S., 2005b. Magnetostratigraphy of the late Cenozoic Laojunmiao anticline in the northern Qilian Mountains and its implications for the northern Tibetan Plateau uplift. Science in China Series D: Earth Sciences 48, 1040–1051.
Fang, X.M., Zhang, W.L., Meng, Q.Q., Gao, J.P., Wang, X.M., King, J., Song, C.H., Dai, S., Miao, Y.F., 2007. High-resolution magneto stratigraphy of the Neogene Huaitoutala section in the eastern Qaidam Basin on the NE Tibetan Plateau, Qinghai Province, China and its implication on tectonic uplift of the NE Tibetan Plateau. Earth and Planetary Science Letters 258, 293–306.
Fang, X.M., Liu, D.L., Song, C.H., Dai, S., Meng, Q.Q., 2012. Oligocene slow and Miocene–Quaternary rapid deformation and uplift of the Yumu Shan and North Qilian Shan: evidence from high-resolution magnetostratigraphy and tectonosedimentology. Geological Society, London, Special Publications 373. http://dx.doi.org/10.1144/SP373.5.
Ford, M., Williams, E.A., Artoni, A., Vergés, J., Hardy, S., 1997. Progressive evolution of a fault-related fold pair from growth strata geometries, Sant Llorenc de Morunys, SE Pyrenees. Journal of Structural Geology 19, 413–441 (Special Issue on Fault-Related Folding).
Gao, H.S., Liu, X.F., Pan, B.T., Wang, Y., Yu, Y.T., Li, J.J., 2008. Stream response to Quaternary tectonic and climatic change: evidence from the upper Weihe River, central China. Quaternary International 186, 123–131.
Garzione, C.N., Ikari, M.J., Basu, A.R., 2005. Source of Oligocene to Pliocene sedimentary rocks in the Linxia Basin in northeastern Tibet from Nd isotopes: implications for tectonic forcing climate. Geological Society of America Bulletin 117, 1146–1155.
Guo, Z.T., Ruddiman, W.F., Hao, Q.Z., Wu, H.B., Qiao, Y.S., Zhu, R.X., Peng, S.Z., Wei, J.J., Yuan, B.Y., Liu, T.S., 2002. Onset of Asian desertification by 22 Myr ago inferred from loess deposits in China. Nature 416, 159–163.
Han, W.X., Fang, X.M., Berger, A., Yin, Q.Z., 2011. An astronomically tuned 8.1 Ma eolian record from the Chinese Loess Plateau and its implication on the evolution of Asian monsoon. Journal of Geophysical Research 116, D24114. http://dx.doi.org/10.1029/2011JD016237.
Harkins, N., Kirby, E., Heimsath, A., Robinson, R., Reiser, U., 2007. Transient fluvial incision in the headwaters of the Yellow River, northeastern Tibet, China. Journal of Geophysical Research 112, F03S04.
Hövermann, J., Süssenberger, H., 1986. Zur Klimageschichte Hoch- und Ostasiens. Berliner Geographische Studie 20, 173–186.
Hui, Z.C., Li, J.J., Xu, Q.H., Song, C.H., Zhang, J., Wu, F.L., Zhao, Z.J., 2011. Miocene vegetation and climatic changes reconstructed from a sporopollen record of the Tianshui Basin, NE Tibetan Plateau. Palaeogeography Palaeoclimatology Palaeoecology 308, 373–382.
Jolivet, M., Brunel, M., Seward, D., Xu, Z., Yang, J., Roger, F., Tapponnier, P., Malavieille, J., Arnaud, N., Wu, C., 2001. Mesozoic and Cenozoic tectonics of the northern edge of the Tibetan plateau: fission-track constraints. Tectonophysics 343 (1–2), 111–134.
Kutzbach, J.E., Guetter, P.J., Ruddiman, W.F., Prell, W.L., 1989. Sensitivity of climate to late Cenozoic uplift in southern Asia and the American west: numerical experiments. Journal of Geophysical Research 94, 18393–18407.
Kutzbach, J.E., Prell, W.L., Ruddiman, W.F., 1993. Sensitivity of Eurasian climates to surface uplift of the Tibetan plateau. Journal of Geology 101, 177–190.
Lease, R.O., Burbank, D.W., Hough, B., Wang, Z., Yuan, D., 2012. Pulsed Miocene range growth in northeastern Tibet: insights from Xunhua Basin magnetostratigraphy and provenance. Geological Society of America Bulletin 124, 657–677.
Li, J.J., 1991. The environmental effects of the uplift of the Qinghai–Xizang Plateau. Quaternary Science Reviews 10, 479–483.
Li, J.J., 1995. Uplift of Qinghai–Xizang (Tibet) Plateau and Global Change.Lanzhou Univ. Press, Lanzhou 207.
Li, J.J., Fang, X.M., 1999. Uplift of Tibetan Plateau and environmental changes. Chinese Science Bulletin 44, 2117–2124.
Li, J.J., Feng, Z.D., Li, T.Y., 1988. Late Quaternary monsoon pattern on the Loess Plateau of China. Earth Surface Processes and Landforms 13, 125–135.
Li, J.J., Fang, X.M., Ma, H.Z., Zhu, J.J., Pan, B.T., Chen, H.L., 1996. Geomorphologic and environmental evolution in the upper reaches of the Yellow River during the Late Cenozoic. Science in China Series D: Earth Sciences 39, 380–390.
Li, J.J., Fang, X.M., Van der Voo, R., Zhu, J.J., MacNiocaill, C., Cao, J.X., Zhong, W., Chen, H.L., Wang, J.L., Wang, J.M., Zhang, Y.T., 1997a. Late Cenozoic magnetostratigraphy (11–0 Ma) of the Dongshanding and Wangjiashan sections in Longzhong Basin, western China. Geologie en Mijnbouw 76, 121–134.
Li, J.J., Fang, X.M., Van der Voo, R., Zhu, J.J., Niocaill, C., Cao, J.X., Zhong, W., Chen, H.L., Wang, J.L., Wang, J.M., Zhang, Y.C., 1997b. Magnetostratigraphic dating of river terraces: Rapid and intermittent incision by the Yellow River of the northeastern margin of the Tibetan Plateau during the Quaternary. Journal of Geophysical Research (D) 102, 10,121–10,132.
Li, J.J., Fang, X.M., Ma, Y.Z., 1998. Sedimentological, geochemical and pollen-spore evidence for a Late Miocene expansion of grasslands/dry climates in Western China. Proc. 30th International Geology Congress. Quaternary Geology, vol. 21, pp. 47–60.
Li, J.J., Zhang, J., Song, C.H., Zhao, Z.J., Zhang, Y., Wang, X.X., Zhang, J.M., Cui, Q.Y., 2006. Miocene Bahean stratigraphy in the Longzhong Basin, northern central China and its implications in environmental change. Science in China Series D: Earth Sciences 49, 1270–1279.
Li, X.R., Fang, X.M., Wu, F.L., Miao, Y.F., 2011. Pollen evidence from Baode of the northern Loess Plateau of China and strong East Asian summer monsoons during the Early Pliocene. Chinese Science Bulletin 56, 64–69.
Liu, T.S., 1985. Loess and the Environment.China Ocean Press, Beijing.
Liu, X.D., Yin, Z.Y., 2002. Sensitivity of East Asian monsoon climate to the uplift of the Tibetan Plateau. Palaeogeography Palaeoclimatology Palaeoecology 183, 223–245.
Lü, L.Q., Fang, X.M., Manson, J.A., Li, J.J., An, Z.S., 2001. The evolution of coupling of Asian winter monsoon and high latitude climate Northern Hemisphere—grain evidence from 8.1 Ma loess–red clay sequence on the Chinese central Loess Plateau. Science in China Series D: Earth Sciences 44, 185–192 (Suppl.).
Ma, Y.Z., Li, J.j, Fang, X.M., 1998. Pollen-spores in the red bed during 30.6–5 Ma in the Linxia Basin and climatic evolution. Chinese Science Bulletin 43, 301–304 (in Chinese).
Ma, Y.Z., Fang, X.M., Li, J.J., Wu, F.L., Zhang, J., 2005a. The vegetation and climate change during Neocene and Early Quaternary in Jiuxi Basin. Science in China Series D: Earth Sciences 48, 676–688.
Ma, Y.Z., Wu, F.L., Fang, X.M., Li, J.J., An, Z.S., Wei, W., 2005b. Pollen record from red clay sequence in the central Loess Plateau between 8.1 and 2.6 Ma. Chinese Science Bulletin 50, 2234–2242.
Manabe, S., Broccoli, A.J., 1990. Mountains and arid climates of middle latitudes. Science 247, 192–194.
Metiver, F., Gaudemer, Y., Tapponnier, P., Meyer, B., 1998. Northeastward growth of the Tibet plateau deduced from balanced reconstruction of two depositional areas: the Qaidam and Hexi Corridor basins, China. Tectonics 17 (6), 823–842.

Meyer, B.P., Tapponnier, L., Bourjot, F., Métivier, Y., Gaudemer, G., Peltzer, S., Guo, Z.C., 1998. Crustal thickening in Gansu–Qinghai, lithospheric mantle subduction, and oblique, strike-slip controlled growth of the Tibet Plateau. Geophysical Journal International 135, 1–47.
Miao, Y.F., Fang, X.M., Herrmann, M., Wu, F.L., Zhang, Y.Z., Liu, D.L., 2011. Miocene pollen record of KC-1 core in the Qaidam Basin, NE Tibetan Plateau and implications for evolution of the East Asian monsoon. Palaeogeography Palaeoclimatology Palaeoecology 299, 30–38.
Molnar, P., 2005. Mio-Pliocene growth of the Tibetan Plateau and evolution of East Asian climate. Palaeontologia Electronica 8 (2A:23 pp., 625 KB).
Molnar, P., Stock, J., 2009. Slowing of India's convergence with Eurasia since 20 Ma and its implications for Tibetan mantle dynamics. Tectonics 28, TC3001. http://dx.doi.org/10.1029/2008TC002271.
Molnar, P., Tapponnier, P., 1975. Cenozoic tectonics of Asia—effects of a continental collision. Science 189, 419–426.
Molnar, P., Boos, W.R., Battisti, D.S., 2010. Orographic controls on climate and paleoclimate of Asia: thermal and mechanical roles for the Tibetan Plateau. Annual Review of Earth and Planetary Sciences 38, 77–102.
Pan, B.T., Li, J.J., Zhu, J.J., Chen, F.H., Cao, J.X., Zhang, Y.T., Cheng, H.L., 1991. Terrace development of Yellow River and gemorphic evolution in Lanzhou area. Quaternary Glacier and Evironment Research in West China. Science Press, Beijing, pp. 271–277 (in Chinese with English Abstract).
Pan, B.T., Li, J.J., Zhou, S.Z., 1992. Discovery of the penultimate glaciation ice-wedge on the Tibetan Plateau and its significance. Chinese Science Bulletin 17, 1599–1602 (in Chinese).
Pan, B.T., Li, J.J., Cao, J.X., Chen, F.H., 1996. Study on the geomorphic evolution and development of the Yellow River in the Hualong Basin. Mountain Research and Development 14, 153–158 (in Chinese with English abstract).
Pan, B.T., Su, H., Hua, Z.B., Hu, X.F., Gao, H.S., Li, J.J., Kirby, E., 2009. Evaluating the role of climate and tectonics during non-steady incision of the Yellow River: evidence from a 1.24 Ma terrace record near Lanzhou. Quaternary Science Reviews 28, 3281–3290.
Perrineau, A., Van der Woerd, J., Gaudemer, Y., Liu, Z.J., Pik, R., Tapponnier, P., Thuizat, R., Zheng, R.Z., 2011. Incision rate of the Yellow River in Northeastern Tibet constrained by ^{10}Be and ^{26}Al cosmogenic isotope dating of fluvial terraces: implications for catchment evolution and plateau building. Geological Society, London, Special Publications 353, 189–219. http://dx.doi.org/10.1144/SP353.10.
Porter, S.C., An, Z.S., 1995. Correlation between climate events in the North Atlantic and China during the last glaciation. Nature 375, 305–308.
Qiang, X.K., An, Z.S., Song, Y.G., Chang, H., Sun, Y.B., Liu, W.G., Ao, H., Dong, J.B., Fu, C.F., Wu, F., 2011. New eolian red clay sequence on the western Chinese Loess Plateau linked to onset of Asian desertification about 25 Ma ago. Science in China Series D: Earth Sciences 54, 136–144.
Rafini, S., Mercier, E., 2002. Forward modeling of foreland basins progressive unconformities. Sedimentary Geology 146, 75–89.
Ramstein, G., Fluteau, F., Besse, J., Joussaume, S., 1997. Effect of orogeny, plate motion and land–sea distribution on Eurasian climate change over the past 30 million years. Nature 386, 788–795.
Rea, D.K., Snoeckx, H., Joseph, L.H., 1998. Late Cenozoic eolian deposition in the North Pacific: Asian drying, Tibetan uplift, and cooling of the north hemisphere. Paleoceanography 13, 215–224.
Ren, S.M., Ge, X.H., Yang, Z.Y., Lin, Y.X., Hu, Y., Liu, Y.J., Genser, J., Rieser, A.B., 2006. An important geological event in northern Qinghai-Tibetan Plateau: constraints from 36Cl dating in western Qaidam Basin. Acta Geologica Sinica 80 (8), 1110–1117.
Royden, L.H., Burchfiel, B.C., van der Hilst, R.D., 2008. The geological evolution of the Tibetan Plateau. Science 321, 1054–1058.
Ruddiman, W.F., Kutzbach, J.E., 1989. Forcing of the late Cenozoic uplift northern hemisphere climate by plateau uplift in the Southern Asia and American West. Journal of Geophysical Research 94, 18409–18427.
Song, Y.G., Fang, X.M., Li, J.J., An, Z.S., Yang, D., Lü, L.Q., 2000. Age of red clay at Chaona section near eastern Liupan Shan and its tectonic significance. Quaternary Science Reviews 20, 457–463 (in Chinese).
Song, C.H., Fang, X.M., Li, J.J., Gao, J.P., Fan, M.J., 2001. Tectonic uplift and sedimentary evolution of the Jiuxi Basin in the northern margin of the Tibetan Plateau since 13 Ma BP. Science in China Series D: Earth Sciences 44, 192–202 (Suppl.).
Song, Y.G., Fang, X.M., Li, J.J., An, Z.S., Miao, X.D., 2001. The late Cenozoic uplift process of Liupan Shan, China. Science in China Series D: Earth Sciences 44, 176–184 (Supplement).
Song, C.H., Fang, X.M., Gao, J.P., Nie, J.S., Yan, M.D., Xu, X.H., Sun, D., 2003. Magnetostratigraphy of Late Cenozoic fossil mammals in the northeastern margin of the Tibetan Plateau. Chinese Science Bulletin 48, 188–193.
Song, C.H., Gao, D.L., Fang, X.M., Cui, Z.J., Li, J.J., Yang, S.L., Jin, H.B., Burbank, D., Kirschvink, J.L., 2005. High-resolution magnetostratigraphy of late Cenozoic sediments from the Kunlun Shan Pass Basin and its implications on deformation and uplift of the northern Tibetan Plateau. Chinese Science Bulletin 50, 1912–1922.
Suppe, J., Chou, G.T., Hook, S.C., 1992. Rate of folding and faulting determined from growth strata. In: McClay, K.R. (Ed.), Thrust Tectonics. Springer, Netherlands, pp. 105–121.
Tapponnier, P., Meyer, B., Avouac, J.P., Peltzer, G., Gaudemer, Y., Guo, S.M., Xiang, H.F., Yin, K.L., Chen, Z.T., Cai, S.H., Dai, H.G., 1990. Active thrusting and folding in the Qilian Shan, and decoupling between upper crust and mantle in northeastern Tibet. Earth and Planetary Science Letters 97 (3–4), 382–383 (387–403).
Tapponnier, P., Xu, Z.Q., Roger, F., Meyer, B., Arnaud, N., Wittlinger, G., Yang, J.S., 2001. Geology—oblique stepwise rise and growth of the Tibet plateau. Science 294, 1671–1677.
Verges, J., Marzo, M., Munoz, J.A., 2002. Growth strata in foreland settings. Sedimentary Geology 146, 1–9.
Wang, J.L., Fang, X.M., Li, J.J., 1999. Eolian sand deposition and its environmental significance in the northeastern margin of the Qinghai–Xizang Plateau. Chinese Science Bulletin 44, 2250–2255.
Wang, X.M., Qiu, Z.D., Li, Q., Wang, B.Y., Qiu, Z.X., Downs, W.R., Xie, G.P., Xie, J.Y., Deng, T., Takeuchi, G.T., 2007. Vertebrate paleontology, biostratigraphy, geochronology, and paleoenvironment of Qaidam Basin in northern Tibetan Plateau. Palaeogeography Palaeoclimatology Palaeoecology 254, 363–385.
Wang, W.T., Zhang, P.Z., Kirby, E., Wang, L.H., Zhang, G.L., Zheng, D.W., Chai, C.Z., 2011a. A revised chronology for Tertiary sedimentation in the Sikouzi basin: implications for the tectonic evolution of the northeastern corner of the Tibetan Plateau. Tectonophysics 505, 100–114.
Wang, X.X., Zattin, M., Li, J., Song, C., Peng, T., Liu, S., Liu, B., 2011b. Eocene to Pliocene exhumation history of the Tianshui–Huicheng region determined by apatite fission-track thermochronology: implication for evolution of the northeastern Tibetan Plateau margin. Journal of Asian Earth Sciences 42, 97–110.
Wang, J.Y., Fang, X.M., Appel, E., Song, C.H., 2012a. Pliocene–Pleistocene climate change at the NE Tibetan Plateau deduced from lithofacies variation in the drill core SG-1, western Qaidam Basin. Journal of Sedimentary Research 82, 933–952.
Wang, X.X., Li, J.J., Song, C.H., Zattin, M., Zhang, J., Zhao, Z., Zhang, Y., 2012b. Late Cenozoic orogenic history of Western Qinling inferred from sedimentation of Tianshui basin, northeastern margin of Tibetan Plateau. International Journal of Earth Sciences 101, 1345–1356. http://dx.doi.org/10.1007/s00531-011-0724-5.
Wu, F.L., Fang, X.M., Ma, Y.Z., An, Z.S., Li, J.J., 2004. A 1.5 Ma sporopollen record of paleoecologic environment evolution in the central Chinese Loess Plateau. Chinese Science Bulletin 49, 295–301.
Wu, F.L., Fang, X.M., Ma, Y.Z., Herrmann, M., Mosbrugger, V., An, Z.S., Miao, Y.F., 2007. Plio-Quaternary stepwise drying of Asia: evidence from a 3-Ma sporopollen record from the Chinese Loess Plateau. Earth and Planetary Science Letters 257, 160–169.
Wu, F.L., Fang, X.M., Herrmann, M., Mosbrugger, V., Miao, Y.F., 2011. Extended drought in the interior of Central Asia since the Pliocene reconstructed from sporopollen records. Global and Planetary Change 76, 16–21.
Xu, S.Y., 1987. Depositional period and sedimentary environment of Gonghe Series in the Qinghai Province, China. Journal of Lanzhou University (Natural Sciences) 23, 109–119 (in Chinese with English abstract).
Yan, M.D., Van der Voo, R., Fang, X.M., Parés, J.M., Rea, D.K., 2006. Paleomagnetic evidence for a mid-Miocene clockwise rotation of about 25° of the Guide Basin area in NE Tibet. Earth and Planetary Science Letters 241, 234–247.
Yan, M.D., Fang, X.M., Van der Voo, R., Song, C.H., Li, J.J., 2012a. Neogene rotations in the Jiuquan Basin, Hexi Corridor, China. Geological Society, London, Special Publications 373. http://dx.doi.org/10.1144/SP373.6.
Yan, M.D., Van Der Voo, R., Fang, X.M., Song, C.H., 2012b. Magnetostratigraphy, fence diagrams and basin analysis. Geological Society, London, Special Publications 373. http://dx.doi.org/10.1144/SP373.3.
Yang, Y.B., Fang, X.M., Appel, E., Galy, A., Li, M.H., Zhang, W.L., 2013. Quaternary paleolake nutrient evolution and climatic change in the western Qaidam Basin deduced from phosphorus geochemistry record of deep drilling core SG-1. Quaternary Research 80, 586–595.
Yin, A., Rumelhart, P.E., Butler, R., Cowgill, E., Harrison, T.M., Foster, D.A., Ingersoll, R.V., Zang, Q., Zhou, X.Q., Wang, X.F., 2002. Tectonic history of the Altyn Tagh fault system in northern Tibet inferred from Cenozoic sedimentation. Geological Society of America Bulletin 114, 1257–1295.
Yue, L., Lei, X., Qu, H., 1991. A magnetostratigraphic study on the Jingyuan loess section, Gansu. China. Quaternary Science Reviews 4, 349–353 (in Chinese with English abstract).
Zachos, J.C., Gerald, R.D., Richard, E.Z., 2008. An early Cenozoic perspective on greenhouse: warming and carbon-cycle dynamics. Nature 451 (17), 279–283.
Zhang, W.L., 2006. Cenozoic Uplift of the Tibetan Plateau: Evidence from High Resolution Magnetostratigraphy of the Qaidam Basin. (PhD thesis) Lanzhou Univesity 1–158 (in Chinese).
Zhang, H.P., Craddock, W.H., Lease, R.O., Wang, W.T., Yuan, D.Y., Zhang, P.Z., Molnar, P., Zheng, D.W., Zheng, W.J., 2012. Magnetostratigraphy of the Neogene Chaka basin and its implications for mountain building processes in the north-eastern Tibetan Plateau. Basin Research 24, 31–50.
Zhang, J., Li, J.J., Song, C.H., Zhao, Z.J., Xie, G.P., Wang, X.X., Hui, Z.C., Peng, T.J., 2013. Paleomagnetic ages of Miocene fluvio-lacustrine sediments in the Tianshui Basin, western China. Journal of Asian Earth Sciences 62, 341–348.
Zhang, Z.G., Han, W.X., Fang, X.M., Song, C.H., Li, X.Y., 2013. Late Miocene–Pleistocene aridification of Asian inland revealed by geochemical records of lacustrine-fan delta sediments from the western Tarim Basin, NW China. Palaeogeography Palaeoclimatology Palaeoecology. http://dx.doi.org/10.1016/j.palaeo.2013.03.008.
Zheng, S.H., Wu, W.Y., Li, Y., 1985. Late Cenozoic mammalian faunas of Guide and Gonghe Basins, Qinghai Province. Vertebrata Palasiatica 23, 89–134 (in Chinese with English abstract).
Zheng, D., Zhang, P., Wan, J., Yuan, D., Li, C., Yin, G., Zhang, G., Wang, Z., Min, W., Chen, J., 2006. Rapid exhumation at 8 Ma on the Liupan Shan thrust fault from apatite fission-track thermochronology: implications for growth of the northeastern Tibetan Plateau margin. Earth and Planetary Science Letters 248, 198–208.
Zheng, D., Clark, M.K., Zhang, P., Zheng, W., Farley, K.A., 2010. Erosion, fault initiation and topographic growth of the north Qilian Shan (northern Tibetan Plateau). Geosphere 6, 937–941. http://dx.doi.org/10.1130/GES00523.1.
Zhu, J.J., Zhong, W., Li, J.J., Cao, J.X., Wang, J.M., Wang, J.L., 1996. The oldest eolian loess deposition in the Longxi Basin–Yandonggou profile in Lanzhou. Scientia Geographica Sinica 16, 365–369 (in Chinese with English Abstract).

https://doi.org/10.1016/j.yqres.2014.01.002 Published online by Cambridge University Press